C. R. Physique 17 (2016) 90–112

Contents lists available at ScienceDirect

Comptes Rendus Physique

www.sciencedirect.com

Iron-based superconductors / Supraconducteurs à base de fer

Electronic nematic susceptibility of iron-based superconductors

Susceptibilité nématique électronique dans les supraconducteurs à base de fer

Anna E. Böhmer [*,1], Christoph Meingast [*]

Institut für Festkörperphysik, Karlsruhe Institute of Technology, 76021 Karlsruhe, Germany

ARTICLE INFO

Article history:
Available online 4 September 2015

Keywords:
Iron-based superconductors
Thermodynamic properties
Mechanical properties

Mots-clés :
Supraconducteurs à base de fer
Propriétés thermodynamiques
Propriétés mécaniques

ABSTRACT

We review our recent experimental results on the electronic nematic phase in electron- and hole-doped $BaFe_2As_2$ and FeSe. The nematic susceptibility is extracted from shear-modulus data (obtained using a three-point-bending method in a capacitance dilatometer) using Landau theory and is compared to the nematic susceptibility obtained from elastoresistivity and Raman data. FeSe is particularly interesting in this context, because of a large nematic, i.e., a structurally distorted but paramagnetic, region in its phase diagram. Scaling of the nematic susceptibility with the spin lattice relaxation rate from NMR, as predicted by the spin-nematic theory, is found in both electron- and hole-doped $BaFe_2As_2$, but not in FeSe. The intricate relationship of the nematic susceptibility to spin and orbital degrees of freedom is discussed.

© 2015 Académie des sciences. Published by Elsevier Masson SAS. All rights reserved.

RÉSUMÉ

Nous présentons dans cette revue nos récents résultats expérimentaux concernant la phase nématique électronique des composés $BaFe_2As_2$ dopés et FeSe. La susceptibilité nématique, extraite de nos mesures du module de cisaillement (obtenue par des essais de flexion trois points par dilatométrie capacitive) dans le cadre de la théorie de Landau, est comparée aux résultats obtenus par des mesures d'élastorésistivité et de spectroscopie Raman. FeSe est un composé particulièrement intéressant dans ce contexte car son diagramme de phase présente une large phase nématique i.e. une phase paramagnétique accompagnée d'une distorsion structurelle. La loi d'échelle reliant la susceptibilité nématique au taux de relaxation spin-réseau observé par RMN, prédite par la théorie nématique de spin, est observée pour les composés $BaFe_2As_2$ dopés en électrons et en trous. La relation complexe entre la susceptibilité nématique et les degrés de liberté orbitaux et de spin est discutée en détail.

© 2015 Académie des sciences. Published by Elsevier Masson SAS. All rights reserved.

* Corresponding authors.
E-mail addresses: anna.boehmer@kit.edu (A.E. Böhmer), christoph.meingast@kit.edu (C. Meingast).
[1] Now at Ames Laboratory/Iowa State University.

http://dx.doi.org/10.1016/j.crhy.2015.07.001
1631-0705/© 2015 Académie des sciences. Published by Elsevier Masson SAS. All rights reserved.

1. Introduction

Electronic nematic phases have recently attracted considerable attention, especially in connection with high-temperature superconductivity [1,2]. For these phases, the term "nematic", which originally refers to a liquid-crystal phase, in which rotational symmetry is broken while translational symmetry is preserved, has been borrowed from its original context to describe a symmetry breaking due to electronic effects [3]. In the iron-based systems, the stripe-type antiferromagnetic phase [4–7], which occurs in close proximity to the superconducting phase, reduces the C_4 rotational symmetry of the high-temperature tetragonal state to C_2 (orthorhombic), which is referred to as Ising-nematic. This breaking of the symmetry is necessarily accompanied by an orthorhombic lattice distortion [8]. Simultaneous magnetic and structural phase transitions occur, for example, in underdoped $Ba_{1-x}K_xFe_2As_2$ [9], suggesting that the small lattice distortion ($\lesssim 4\times10^{-3}$) is simply induced by magnetoelastic coupling. However, it was observed early on that the (nearly [10]) concomitant magneto-structural phase transition of the parent compound $BaFe_2As_2$ splits into two well-defined transitions upon Co substitution [11,12]. Neutron diffraction studies demonstrated that the structural transition temperature T_s is several K higher than the magnetic transition temperature T_N [13,14]. Hence, there is a small region of an orthorhombic—i.e., "nematic"—but paramagnetic phase in $Ba(Fe_{1-x}Co_x)_2As_2$, which is also observed, e.g., in other transition-metal-doped 122-systems [15], in F-doped 1111-compounds [16], and in Co-doped NaFeAs [17]. Intuitively, $T_s > T_N$ suggests that the structural instability is the primary one, even though scenarios in which the structural transition is nevertheless a consequence of magnetic interactions have been proposed soon after [18–21]. The observation certainly puts the simple picture of the orthorhombic distortion as a mere consequence of stripe-type antiferromagnetism into question and has sparked great interest in the nematic phase of the iron-based materials, including an intensive debate about its microscopic origin [2]. Of particular interest in this debate is FeSe, which undergoes a similar structural distortion as the other compounds, but does not order magnetically [22].

Here we review and discuss our recent measurements of the elastic shear modulus, which is shown to be a particularly sensitive probe of the incipient structural distortion and, hence, nematicity. In particular, we measured Young's modulus using a novel three–point-bending setup in a capacitance dilatometer [23,24]. Young's modulus along a specific direction is shown to reflect the shear modulus, which is the soft mode of the structural transition, i.e., it is expected to vanish at the transition. Assuming the existence of an electronic nematic order parameter driving the transition, as indicated by elastoresistivity measurements [25], the electronic nematic susceptibility can be inferred using a simple Landau theory. Results on three iron-based systems—electron-doped $Ba(Fe_{1-x}Co_x)_2As_2$, hole-doped $(Ba_{1-x}K_x)Fe_2As_2$ and FeSe—are discussed and compared. These thermodynamic measurements alone cannot determine the origin (spin or orbital, localized or itinerant interactions) of the nematic susceptibility. We therefore compare our results with probes of the charge (electronic Raman scattering) and spin (nuclear magnetic resonance, NMR) degrees of freedom. In particular, we test a scaling relation of the nematic susceptibility with magnetic fluctuations, which are derived from NMR data. This scaling relation is obtained within the itinerant spin-nematic scenario [26], in which the structural transition is a direct consequence of strong magnetic fluctuations. Throughout the article, we use the notation of the two-iron (or the tetragonal) unit cell, in which the structural distortion occurs in the B_{2g} channel and is related to the elastic shear modulus C_{66} and Young's modulus $Y_{[110]}$.

The contribution is organized as follows. In the remaining part of this Introduction, we review previous experimental and theoretical works on nematicity, in particular as related to the softening of the shear modulus C_{66} above the structural transition. In the following, we detail how C_{66} can be linked to the nematic susceptibility using Landau theory (Section 2). In Section 3 we present briefly the three-point-bending technique and in Section 4 we show how the elastic data is influenced by domain formation in the orthorhombic state using dynamical three-point-bending measurements on $BaFe_2As_2$. In Section 5 we present comprehensive shear-modulus data of $Ba(Fe_{1-x}Co_x)_2As_2$ and $(Ba_{1-x}K_x)Fe_2As_2$ [23] and of FeSe [27]. The inferred nematic susceptibility of FeSe is shown to be remarkably similar to the one of underdoped $BaFe_2As_2$. Section 6 presents the comparison of our elastic data to elastoresistivity measurements and electronic Raman scattering. In Section 7 we show the scaling of the shear modulus with magnetic fluctuations, derived from NMR data, discussed within the itinerant spin-nematic scenario. This scaling is found to be well satisfied in both $Ba(Fe_{1-x}Co_x)_2As_2$ [26] and $(Ba_{1-x}K_x)Fe_2As_2$, but seems to fail for FeSe. Finally, we present a summary and outlook in Section 8.

1.1. Electronic in-plane anisotropy

The anisotropic properties of the magnetic/nematic phase have been studied by various experimental techniques. An early observation of electronic in-plane anisotropy in the orthorhombic phase was a large $a-b$ anisotropy of the resistivity in $Ba(Fe_{1-x}Co_x)_2As_2$ (nearly a factor of 2) [28]. However, it was subsequently shown experimentally that this resistivity anisotropy strongly depends on the degree of disorder of the samples and the type of substitution [29–34]. Various theoretical works also place emphasis on the role of disorder in explaining these observations [35,33,36]. Strongly anisotropic defects in the orthorhombic state, which are a candidate to produce this resistivity anisotropy, were, indeed, observed using scanning tunneling microscopy [37–39] and recent measurements of the anisotropy of the Hall effect also point to a dominating role of the carrier mobility anisotropy in creating the resistivity anisotropy [40]. However, optical conductivity studies show the importance of orbital anisotropy in addition to the anisotropy of scattering rates [41,30,42,43]. A recent work [44] stresses, in particular, the importance of the anisotropy of the Drude weight, rather than scattering rate, for the resistivity

anisotropy, as was also indicated by disorder-dependent elastoresistivity measurements [45]. Similarly, early angle-resolved photo-emission spectroscopy (ARPES) measurements found a significant shift of the d_{xz} (d_{yz}) orbitals to lower (higher) energies below T_s [46], i.e., orbital order. These results have been addressed in various theoretical works [47–49]. Further, the thermopower was shown to have an even larger anisotropy than the resistivity in the orthorhombic state, arising from an interplay of anisotropic scattering and orbital polarization [50]. Nuclear magnetic resonance (NMR) [51] and inelastic neutron scattering studies [52,53] show significant anisotropy of the spin dynamics also in the temperature region $T_s > T > T_N$. Inelastic neutron scattering as a probe of nematicity is described in another contribution to this issue [54]. Altogether, the observed large electronic anisotropy in the presence of a rather small lattice distortion of $\delta = (a-b)/(a+b) < 0.4\%$ supports the idea that an electronic order parameter, which has to be "nematic" by symmetry, drives the structural transition. To show this, the resistivity anisotropy induced by an externally imposed lattice distortion (applied to a sample via a piezo stack) was measured in Ref. [25]. It was found that, indeed, the susceptibility of an electronic nematic order parameter diverges on approaching T_s from above, in agreement with the assumption that it drives the structural transition. Similarly, a study of the electronic relaxation dynamics using femtosecond-resolved polarimetry suggests that nematicity is an independent electronic degree of freedom [55].

In order to measure the in-plane anisotropy of various physical quantities, the crystals need to be detwinned, which can be accomplished by the application of a uniaxial stress along the tetragonal [110] direction, $\sigma_{[110]}$ [28,56] or, in some cases, by a high magnetic field [57,58]. An earlier review on detwinning and electronic in-plane anisotropy in the iron-based superconductors is given in Ref. [56]. However, the application of $\sigma_{[110]}$ also significantly smears out the structural transition and can induce a marked anisotropy of electronic properties even above T_s [28,59–62]. This strong sensitivity of the system to $\sigma_{[110]}$ already demonstrates a large nematic susceptibility and can be used to determine it quantitatively. The nematic susceptibility has been evaluated by various techniques, including the above-described strain-dependent resistivity [25], the stress-dependent optical reflectivity [42], the elastic shear modulus [23] and the Raman response [63].

1.2. Two theoretical scenarios—spins vs. orbitals

As to which electronic degrees of freedom, spin or orbital, underlie this electronic nematic order parameter, two main scenarios have been discussed. The first one [64–66] places emphasis on orbital degrees of freedom, in particular the iron d_{xz} and d_{yz} orbitals, which are degenerate in the high-symmetry tetragonal phase. The structural transition, in this scenario, occurs when these orbitals order and become inequivalent in energy. The nematic order parameter φ is then given by the difference in orbital occupation. Orbital order may trigger a secondary magnetic transition [64]. This model naturally explains why the structural transition occurs at a higher temperature than the magnetic transition, yet a magnetic transition does not necessarily follow the structural one within this orbital scenario.

On the other hand, magnetism is essential in the second scenario, where spin fluctuations are considered as the driving force for the structural transition. In this spin-nematic scenario, of which there is a localized [18,19] and an itinerant formulation [21,20,3], the primary instability is that of the stripe–type magnetic phase, with the ordering vector either $Q_1 = (\pi, 0)$ or $Q_2 = (0, \pi)$, in orthorhombic notation. This state has an additional degree of freedom with respect to, e.g., checkerboard-type antiferromagnetism, namely the orientation of the ferromagnetic stripes (i.e., whether the ordering vector is Q_1 or Q_2), and this is determined by the "spin-nematic" order parameter φ [21]. The calculations of Refs. [18,19,21] have shown that φ, and thus the orthorhombic distortion, can be finite at a higher temperature than the magnetic ordering temperature, explaining the observed sequence of phase transitions. The debate about whether orbital or magnetic degrees of freedom are "in the driver's seat" of the structural transition has been reviewed in Ref. [2].

1.3. Extreme cases: orthorhombic distortion without magnetic order in FeSe and tetragonal magnetic phase in hole-doped $BaFe_2As_2$

In most iron-based materials, the onsets of magnetic ordering and the structural distortion occur very close to each other in the phase diagram, which indicates that they are strongly coupled and hampers the determination of the "driver" [2]. There are, however, two exceptions to this which have recently attracted a lot of attention. The first exception is the 11-type iron-based superconductor FeSe, which undergoes a tetragonal-to-orthorhombic structural phase transition at $T_s \sim 90$ K, similar to that found in the underdoped 122 materials and with similar magnitude of the orthorhombic distortion [67,22,27]. Yet, whereas this transition always occurs in proximity to stripe-type antiferromagnetic order in the 122 systems, no static magnetism was found in FeSe at ambient pressure [22,68]. However, an enhanced spin–lattice relaxation rate in NMR at low temperatures indicates the presence of strong spin fluctuations [69]. In contrast to the 122-type systems, phase-pure superconducting FeSe cannot be obtained by self-flux growth techniques. Recently however, high-quality single crystals were obtained using low-temperature vapor transport [70] or $KCl/AlCl_3$ flux [71,72], enabling a multitude of experimental studies including those of Young's modulus, NMR, elastoresistivity, ARPES and inelastic neutron scattering [27,73–79].

FeSe has a rich temperature–pressure phase diagram [67,80–82], which has recently been obtained in new comprehensiveness using resistivity measurements [83,84]. The structural transition is found to be suppressed by hydrostatic pressure at $\lesssim 2$ GPa. On the other hand, the low-temperature spin fluctuations are enhanced by pressure [69] and probably static magnetic order sets in above ~ 1 GPa, with a subsequent increase in the value of T_N [68,81,83]. T_c has a non-monotonic pressure dependence, increasing initially and reaching a local maximum at ~ 0.8 GPa followed by a slight decrease [81–83].

At higher pressures, T_c increases again and the onset of T_c reaches surprisingly 37 K at ~ 7 GPa [85,86,67,80]. Recent inelastic neutron powder [78] and single-crystal [79] diffraction results suggest that magnetic fluctuations at ambient pressure occur around the same $(\pi, 0)$ stripe-type wave vector as in the other iron-based compounds. These puzzling results have recently attracted considerable attention and have resulted in various theoretical scenarios [87–91].

The second exception where magnetic order and orthorhombic distortion do not closely follow each other is the C_4-symmetric reentrant magnetic phase in Na-doped $BaFe_2As_2$ [92]. Within a certain range of Na content, the usual orthorhombic distortion first develops with the stripe-type magnetic order below T_N, but then suddenly disappears within experimental resolution upon entering this phase. This observation was taken as evidence that magnetic degrees of freedom drive the structural phase transition (the spin-nematic scenario) because the existence of such a phase can hardly be reconciled with orbital order being a prerequisite for magnetism [92]. Yet, the detailed magnetic structure is still under intense study. Polarized neutron scattering indicates a spin-reorientation from in-plane to c-axis oriented and suggests that the magnetic structure might still be orthorhombic, while a truly tetragonal "2-Q" magnetic structure could not be ruled out [93]. Group theoretical analysis suggests that the question of who is in the driver's seat may be solved by determining the pattern of magnetic and orbital order within this phase [94]. Further theoretical works [95,96] show that interplay between the two stripe-type magnetic ordering vectors $Q_1 = (0, \pi)$ and $Q_2 = (\pi, 0)$ can lead to the observed phase diagram. This putatively tetragonal magnetic phase was also reported in Na-doped $SrFe_2As_2$ [97] and in single crystals of K-doped $BaFe_2As_2$ [98], where the interplay with superconductivity was also studied. Measurements of the orthorhombic order parameter using capacitance dilatometry [98] of these samples yield an upper limit for the orthorhombic distortion of $\sim 0.01 \times 10^{-3}$ in the new magnetic phase of $Ba_{1-x}K_xFe_2As_2$, i.e. less than 1% of the value of δ in the stripe-type magnetic phase.

1.4. The elastic shear modulus—soft mode of the structural transition

It is clear that once a material undergoes the structural transition, all properties (e.g., lattice constants, orbital occupation or spin fluctuations) acquire in-plane anisotropy, which makes it difficult to distinguish between the two scenarios. As an alternative, the study of the susceptibility of the various quantities above the structural transition has been suggested as a possible viable approach to determine the driving force of the structural transition [25,26,2].

In proximity to the structural phase transition of the iron-based materials (which can be classified as pseudo-proper ferroelastic [99,25]), the elastic shear modulus C_{66} is expected to grow soft. C_{66} was studied extensively in the $Ba(Fe_{1-x}Co_x)_2As_2$ system using ultrasound [21,100,101,66,102], and these measurements indeed show that C_{66} is the soft mode of the structural transition, as expected from the symmetry of the lattice distortion. An ultrasound study on single-crystalline FeSe [103] shows the same soft mode. Further, signatures of a behavior that was termed "structural quantum criticality" were found around optimal doping in the $Ba(Fe_{1-x}Co_x)_2As_2$ system. Namely, the temperature and doping dependence of the structural susceptibility $S_{66} = C_{66}^{-1}$, the inverse of the shear modulus, was found to resemble closely the magnetic susceptibility in proximity to a magnetic quantum critical point [101]. The elastic softening persists over a large part of the superconducting dome on the overdoped side, which makes the associated fluctuations a possible candidate for the pairing glue in the iron-based systems [23,65]. A pronounced hardening of C_{66} below the superconducting transition temperature T_c in optimally doped $Ba(Fe_{1-x}Co_x)_2As_2$ was shown to reflect the competition between magnetism and superconductivity, because the structural distortion and magnetism are strongly coupled in this system [21].

2. Landau theory with bilinear strain-order parameter coupling

In the Landau theory of a second-order phase transition, a structural distortion can be induced by a bilinear coupling in the free energy between elastic strain ε and the primary (possibly electronic) order parameter φ. In the case of the iron-based materials, the structural distortion is given by $\delta = (a-b)/(a+b)$, or $\varepsilon_6 = \frac{\partial u_x}{\partial y} + \frac{\partial u_y}{\partial x}$, the relevant component of the elastic strain tensor, and φ is the electronic nematic order parameter. Note that the bilinear coupling between ε_6 and φ is, indeed, only allowed if φ is "nematic", i.e. if it breaks the four-fold rotational symmetry of the high-temperature phase. However, this phenomenological approach is independent of the microscopic origin of φ (spin or orbital). Due to the bilinear coupling, ε_6 is a measure of φ, i.e. the two quantities are proportional to each other [21]. The stress–strain relation $\sigma_6 = C_{66}\varepsilon_6$ in the tetragonal or orthorhombic system shows that the soft elastic mode is C_{66}, i.e. a second-order structural phase transition occurs when $C_{66} \to 0$.

The relation between the nematic susceptibility and C_{66} can be obtained by considering the free energy density [21,8,25]

$$F = F_0 + \frac{1}{2}C_{66,0}\varepsilon_6^2 - \lambda\varepsilon_6\varphi + \frac{1}{2}\left(\chi_\varphi\right)^{-1}\varphi^2 + \frac{B}{4}\varphi^4 \tag{1}$$

Here, $-\lambda\varepsilon_6\varphi$ is the bilinear coupling term (with the coupling constant λ), $\frac{1}{2}C_{66,0}\varepsilon_6^2$ is the bare elastic energy (*i.e.* without the coupling λ) and $C_{66,0}$ is the bare elastic constant, which, by assumption, has no strong temperature dependence. The last two terms represent a Landau expansion in the nematic order parameter φ, with χ_φ the bare nematic susceptibility and $B > 0$ the usual quartic coefficient of the Landau expansion. A second bilinearly coupled (nematic) order parameter can be included analogously to describe, e.g., the interplay between elastic, spin-nematic and orbital degrees of freedom,

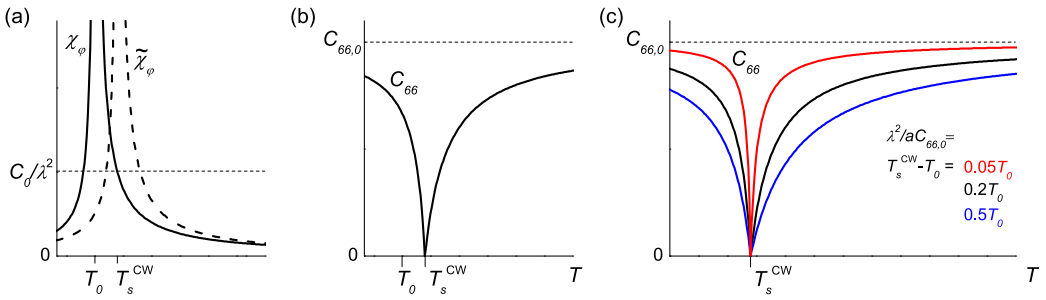

Fig. 1. (a) Temperature dependence of the nematic susceptibility $\chi_\varphi = 1/a(T - T_0)$ (solid line) and the nematic susceptibility renormalized by bilinear coupling to the lattice $\tilde{\chi}_\varphi = 1/a(T - T_s^{CW})$ (dashed line) in a mean-field model. (b) Temperature dependence of the soft elastic mode $C_{66} = (T - T_s^{CW})/(T - T_0)$ of the structural transition induced by this bilinear coupling between the strain component ε_6 and the nematic order parameter φ, Eq. (1). The effect of the bilinear coupling is to increase the transition temperature from T_0 to T_s^{CW}. (c) shows the temperature dependence of C_{66} for a range of parameters $\lambda^2/aC_{66,0} = T_s^{CW} - T_0$. The slope of C_{66} just above T_s is determined by the bilinear coupling strength λ.

as in Refs. [104,105]. Here, however, we restrict ourselves to only one nematic order parameter. In general, the effective, renormalized elastic constant C_{66} is given by [106,107]

$$C_{66} = \frac{\mathrm{d}^2F}{\mathrm{d}\varepsilon_6^2} = \frac{\partial^2 F}{\partial \varepsilon_6^2} - \left(\frac{\partial^2 F}{\partial \varepsilon_6 \partial \varphi}\right)^2 \left(\frac{\partial^2 F}{\partial \varphi^2}\right)^{-1} \tag{2}$$

because the condition that F is minimal with respect to both ε_6 and φ couples the two order parameters. This results in [8,25]

$$C_{66} = C_{66,0} - \frac{\lambda^2}{(\chi_\varphi)^{-1} + 3B\varphi^2} \tag{3}$$

which reduces to $C_{66} = C_{66,0} - \lambda^2 \chi_\varphi$ above the ordering temperature when $\varphi = 0$. Note that χ_φ is also renormalized by the coupling λ and the effective nematic susceptibility $\tilde{\chi}_\varphi$ is given by $(\tilde{\chi}_\varphi)^{-1} = (\chi_\varphi)^{-1} - \lambda^2/C_{66,0}$. Rewriting C_{66} in terms of $\tilde{\chi}_\varphi$, yields the expression of Ref. [21]:

$$\frac{1}{C_{66}} = \frac{1}{C_{66,0}} + \frac{\lambda^2}{C_{66,0}^2}\tilde{\chi}_\varphi \tag{4}$$

Note that Eq. (4) is not limited to a Landau expansion in φ and is actually valid more generally, as long as bilinear coupling to a harmonic lattice is considered [21]. Eqs. (3) and (4) show that we can access the nematic susceptibility χ_φ and also $\tilde{\chi}_\varphi$ by measuring C_{66}.

Before analyzing real data, we illustrate the expected behavior of the shear modulus in the above Landau theory. We assume a mean-field Curie–Weiss-type divergence of χ_φ on approaching T_0, which would be the transition temperature in the absence of coupling to the elastic strain,

$$\chi_\varphi = \frac{1}{a(T - T_0)} \tag{5}$$

This leads to the temperature dependence of the soft elastic mode in a mean-field case [107],

$$C_{66} = C_{66,0}\left(\frac{T - T_s^{CW}}{T - T_0}\right) \quad \text{for } T > T_s^{CW} \tag{6}$$

$$C_{66} = C_{66,0}\left(\frac{2(T_s^{CW} - T)}{3T_s^{CW} - T_0 - 2T}\right) \quad \text{for } T < T_s^{CW} \tag{7}$$

shown in Fig. 1, with $T_s^{CW} = T_0 + \frac{\lambda^2}{aC_{66,0}}$ the new transition temperature, increased with respect to T_0 by the coupling to the strain. An energy scale characteristic of the coupling is given by $T_s^{CW} - T_0$, and determines the curvature of $C_{66}(T)$ in Fig. 1(b, c). Note that the renormalized $\tilde{\chi}_\varphi = 1/a(T - T_s^{CW})$ naturally diverges at the new transition temperature.

In principle, the structural transition may arise either from a divergence of χ_φ, as in an electronically-driven transition, or from a vanishing of $C_{66,0}$, as in a bare lattice instability. It has been proposed that the temperature dependence of C_{66} close to the phase transition can distinguish the two cases [8,107]. Namely, in the Landau theory of a purely elastic transition, the elastic modulus is expected to vanish linearly, since it is the inverse linear susceptibility of the elastic strain. However, for an electronically-driven transition, which is assumed in Eq. (1), the elastic modulus is expected to vanish with a curvature,

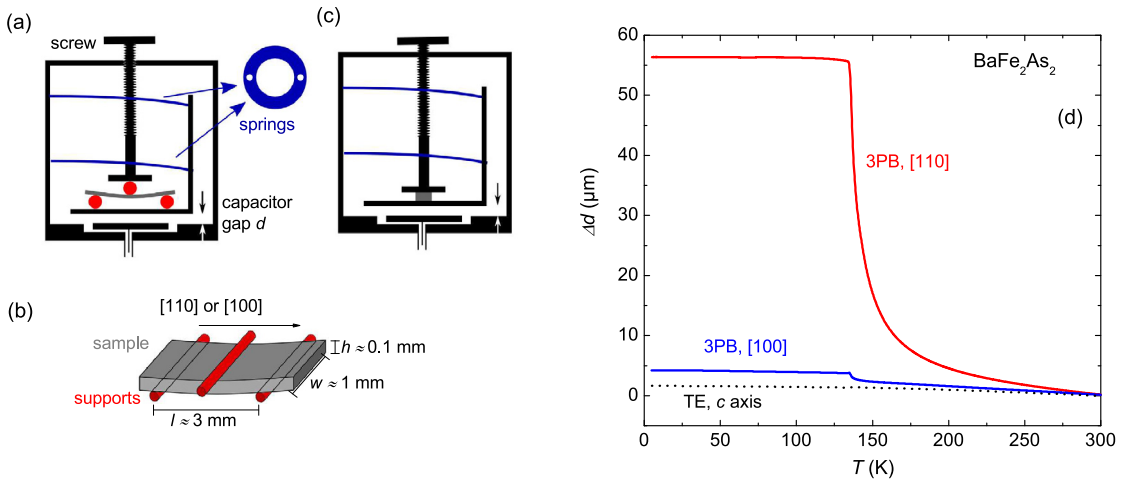

Fig. 2. (a) Schematic representation of the capacitance dilatometer with a sample inserted for three-point bending. The sample (see panel (b), of dimensions $l \times w \times h \approx 3 \times 1 \times 0.1$ mm^3) is supported by three wires and pressed against one movable plate of a plate-type capacitor using a screw with a force of ≈ 0.2 N. The movable capacitor plate is suspended via a set of circular parallel springs and the change of the capacitor gap d (indicated by arrows) on changing temperature is measured. (c) shows the regular setup with a sample inserted for thermal expansion measurement. (d) Temperature evolution of the capacitor gap $d(T)$, expected in a c-axis thermal-expansion (TE) experiment of a 0.1-mm-thick $BaFe_2As_2$ sample [114] (black dashed line), and measured in three-point bending (3PB) of such a sample oriented along [100] (blue line) and [110] (red line). An exceedingly large effect is observed in the latter case, a result of the strong temperature dependence of the shear modulus C_{66} of $BaFe_2As_2$.

following Eq. (6) (Fig. 1). The experimental data, shown below, support the second scenario of an electronic nematic order parameter.

Equation (1) above, however, is limited to a description of a second-order nematic/structural transition and neglects the subsequent (or concomitant) magnetic transition occurring in most iron-based systems. To illustrate the expected temperature dependence of C_{66} for $BaFe_2As_2$, the Landau model can be expanded to describe this split magneto-structural transition phenomenologically. This is achieved by the free energy density

$$F = F_0 + \frac{a}{2}(T - T_0)\varphi^2 + \frac{B}{4}\varphi^4 + \frac{C_{66,0}}{2}\varepsilon_6^2 - \lambda\varepsilon_6\varphi - \varepsilon_6\sigma + \frac{u}{2}(T - T_{N,0})M^2 + \frac{v}{4}M^4 - \mu\varphi M^2 \tag{8}$$

which is equivalent to Eq. (1) concerning the elastic and nematic contributions and adds a magnetic order parameter M. Additionally, the contribution of conjugated uniaxial stress $-\varepsilon_6\sigma$ is also included to model the behavior under finite stress. Parameters values $a = 1$, $T_0 = 1.025$, $B = 1$, $C_{66,0} = 1$, $\lambda = 0.2$, $u = 1$, $T_{N,0} = 1$, $v = 1$ and $\mu = 0.2$ were fine-tuned so that the model reproduces the second-order structural and a first-order magnetic transition slightly below the structural one. Note that the coupling between M and φ causes the magnetic transition to be first order despite a positive fourth-order coefficient v. A solution that minimizes F is calculated numerically for varying values of σ and is shown together with the resulting elastic modulus, C_{66} (still given by Eq. (3) in Fig. 3(b)). Note that the temperature dependence of C_{66} is unchanged with respect to the solution to Eq. (1) in the high-temperature region where $M = 0$, while the first-order transition at T_N induces a step-like hardening of C_{66} on decreasing T.

We note that the above Landau formalism is a mean-field treatment, in which fluctuations of the order parameter are ignored. In fact, this often turns out to be a good approximation for second-order structural phase transitions, because the long-range elastic interactions strongly suppress fluctuations [108–110].

3. Technique: three-point bending in a capacitance dilatometer

Three-point bending is a long-standing and widely used mechanical test to study elastic properties of diverse materials. The technique is particularly appealing by its simplicity. A platelet- or beam-shaped sample is supported along two lines, while a force is applied at a third, middle, line and the induced deflection is measured. Small forces result in a sizable deflection so that the elastic modulus can be measured comparatively easily. In the limit of thin samples, the measured elastic modulus is proportional to the material's Young modulus, which also determines the sample stiffness in a uniaxial tension/compression experiment [111], even though samples are subject to non-uniform stress in three-point bending [112]. We have developed a three-point bending setup in a capacitance dilatometer [113] to measure the Young modulus of iron-based materials with very high resolution [23]. The advantage of this technique over the ultrasound measurements used more traditionally to determine elastic constants is that the sample requirements are not as stringent. In particular, ultrasound velocity measurements require samples of considerable size and quality. On the other hand, the typically quite thin platelet-like single crystals available for the iron-based materials are perfectly suited for the three-point-bending technique. This has allowed us to investigate a larger variety of materials than would have been possible using ultrasound.

In a typical capacitance dilatometer, the sample is held in place by a small uniaxial force from the two-leaf springs of the parallelogram arrangement holding the movable capacitor plate (see Fig. 2(c)). Hence, sample length changes (due to, e.g., thermal expansion) lead to a change in the capacitor gap d. A very high length resolution of 0.1–0.01 Å can be achieved by measuring the resulting change of capacitance [113]. By placing a sample in three-point-bending configuration (Fig. 2(b)) into the dilatometer, as shown in Fig. 2(a), one no longer measures the thermal expansion of the sample, but rather its elastic bending modulus. This is because the small force from the dilatometer causes the sample to bend and the effective height of the arrangement is determined by the sample's flection, hence, its elastic modulus. Notably, when the elastic modulus of such a sample becomes soft (i.e. decreases), the sample bends more strongly, so that its effective height along the axis of the dilatometer decreases. Fig. 2(d) shows examples of such measurements. The red and the blue curves show three-point-bending experiments with samples oriented with their tetragonal [110] and [100] directions, respectively, perpendicular to the supports. An exceedingly large effect is observed in three-point bending along [110]. This is because Young's modulus along [110],

$$Y_{[110]} = 4\left(\frac{1}{C_{66}} + \frac{1}{\gamma}\right)^{-1} \text{ with } \gamma = \frac{C_{11}}{2} + \frac{C_{12}}{2} - \frac{C_{13}^2}{C_{33}} \tag{9}$$

is dominated by the elastic shear modulus C_{66} as long as C_{66} is smaller than the other C_{ij}, and C_{66} decreases strongly on cooling towards T_s [101]. In contrast, the black dashed line shows the much smaller temperature-dependent change in the capacitance gap Δd expected from just the thermal expansion of a 100-µm-thick sample of $BaFe_2As_2$ [114]. A detailed description of the quantitative analysis of the data is given in [24]. The technique is particularly well suited to access large changes in the Young modulus of a sample occurring over a broad temperature range, as well as any sharp anomalies. As we will show, this technique even has the resolution to detect the often very small anomalies at the onset of superconductivity.

In addition to the static three-point-bending measurements in the capacitance dilatometer, ultralow-frequency dynamic three-point-bending measurements of $BaFe_2As_2$ were performed using a Diamond DMA (dynamical mechanical analyzer) from PerkinElmer [115]. Here, samples are subjected to a force $F = F_S + F_D \exp(i\omega t)$ with a dynamic component at the very low frequency of 1 Hz. From the measured displacement $u = u_S + u_D \exp(i(\omega t - \delta))$, the dynamic stiffness $k_s = F_D/u_D \exp(i\delta) \propto Y_{[110]}$ is calculated. k_s may be a complex number in the presence of dissipation, and its real part corresponds to the results of the static measurements.

4. Dynamical three-point-bending measurements of $BaFe_2As_2$

Before addressing the detailed static measurements of Young's modulus in a capacitance dilatometer, we show in this section results of dynamic three-point-bending experiments on $BaFe_2As_2$, which elucidate the role of structural twins in the ordered phase [116]. For these measurements the sample is subjected to the force $F = F_S + F_D \exp(i\omega t)$ with a dynamic component $F_D \sim (0.7\text{–}0.8)F_S$ at a frequency of $\omega/2\pi = 1$ Hz. Fig. 3(a) shows the real part of the Young modulus $Y'_{[110]}$ (equivalent to the result of static measurements) for different F_S but constant ratio F_D/F_S.

A smooth softening of $Y_{[110]}$ upon cooling towards the structural transition is observed (Fig. 3(a)), in agreement with the soft-mode behavior shown in Fig. 1. However, at the lowest stress, a kink and a small, sharp, minimum may be ascribed to the structural and magnetic transition, respectively, and $Y_{[110]}$ is essentially temperature independent below T_N, in strong contrast to the behavior shown in Fig. 1. With increasing stress, the data deviate from the low-stress curve below some $T > T_s$ and $Y_{[110]}$ does not soften as much in total. The structural transition is smeared out, while the magnetic transition is affected much less. Notably, a discontinuous hardening of the Young modulus on cooling through T_N emerges with increasing stress. It is reminiscent of the phonon modes measured using inelastic neutron scattering [117]. At the highest stress, $Y_{[110]}$ indeed recovers its initial high-temperature value at $\sim 0.9\,T_N$. Note that the deviation of this curve from the others at higher temperatures is an experimental artefact.

The experimental data at high stress are well reproduced by the model in Eq. (8) of a split magneto-structural transition (Fig. 3(b)). However, the experimental data obtained at lower stress are much too small in comparison to this model for temperatures $T < T_s$. These anomalously low values of Young's modulus below T_s and at low stress likely arise from the "superelastic" behavior of the twinned samples, which is due to domain wall motion and is typically found in ferroelastic materials [111,118,119]. The effect can be understood by considering two kinds of structural domains, '+'-type domains that are elongated along [110] and '−'-type domains that are shortened along this direction. Application of a small compressive stress $\sigma_{[110]}$ increases the fraction of '−'-type domains at the expense of the '+'-type domains, so that the total sample length decreases through domain wall motion. A relatively small applied force can thus induce significant length changes, which means that the elastic modulus appears very small at low frequencies. In the three-point-bending experiment, samples are essentially subjected to stress along the [110] direction, which suppresses domain formation and leads to a strong variation of the measured $Y_{[110]}$ with applied stress. The true monodomain elastic properties of the system can only be obtained in these dynamic three-point bending experiments if the applied stress is strong enough to force the system into a single domain state.

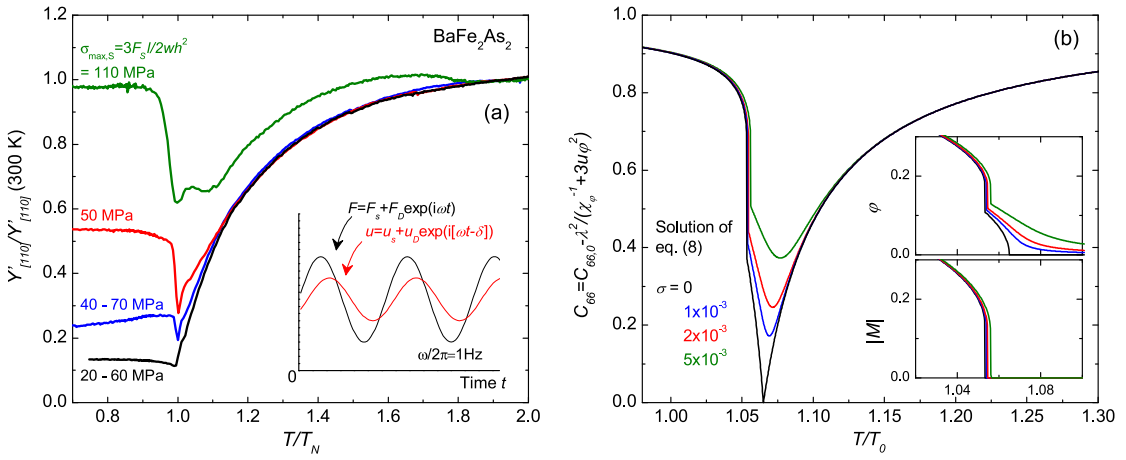

Fig. 3. (a) Real part of the Young modulus $Y'_{[110]}$ of $BaFe_2As_2$ obtained in dynamic three-point-bending experiments in which the applied force $F = F_S + F_D \exp(i\omega t)$ varies at a frequency of $\omega/2\pi = 1$ Hz (see inset). $Y_{[110]} \propto F_D/u_D \exp(i\delta)$ is calculated from the measured displacement $u = u_S + u_D \exp(i(\omega t - \delta))$ under the applied force F (see inset). Data are taken at different F_S and constant ratio F_D/F_S. The maximal uniaxial stress at the sample surface arising from F_S, $\sigma_{max,S} = \frac{3F_S l}{2wh^2}$ [112] is given as a characteristic parameter. The two measurements with the lowest force were conducted in "constant amplitude" mode, in which F_S and F_D are smaller when the sample is soft and increase when the sample becomes harder, thus increasing the resolution. (b) Soft elastic mode in a mean-field picture for closely spaced structural and magnetic phase transitions, obtained via numerically minimizing Eq. (8) (see text for parameters) and then calculating C_{66}. Good agreement with the experimental data is obtained for the high-stress measurement, while the measurements at lower stress and below T_s are dominated by the effect of structural twins. Insets show the order parameters φ and $|\mathbf{M}|$ of the numerical solution.

5. Young's modulus of $Ba(Fe,Co)_2As_2$, $(Ba,K)Fe_2As_2$ and FeSe

Fig. 4 shows Young's modulus $Y_{[110]}$ of Co- and K-doped $BaFe_2As_2$ and of FeSe, as measured by the three-point-bending technique in a capacitance dilatometer described in Section 3 [23,27]. Fig. 4(c) shows that the temperature dependence of $Y_{[110]}$ obtained by three-point bending is very similar to C_{66} (see Eq. (9)) as determined by ultrasound measurements for $Ba(Fe_{1-x}Co_x)_2As_2$ [101], the system for which such data is available. Notably, all essential features of C_{66} are also observed in Young's modulus data, confirming the capacity of our experiment to determine the temperature dependence of the shear modulus. In $BaFe_2As_2$, strong softening of $Y_{[110]}$ upon approaching the transition at T_s from above is observed. The softening gradually disappears with both Co- and K-doping. Interestingly, the Young modulus $Y_{[110]}$ of FeSe, which undergoes a similar structural transition as the iron-arsenides but no magnetic phase transition, shows the same pronounced softening on cooling towards $T_s \approx 90$ K as underdoped $BaFe_2As_2$ (Fig. 4(d)). Contrary to expectations, $Y_{[110]}$ does not reach zero even at the second-order structural phase transitions. The reason for this is unclear at present and may be related to effects of disorder or finite stress. We note that, similarly, C_{66} does not reach zero in the ultrasound data, either. For moderately overdoped samples, a marked softening on cooling is still observed, while $Y_{[110]}$ hardens considerably below T_c. Young's modulus of a non-superconducting, strongly overdoped $Ba(Fe_{0.67}Co_{0.33})_2As_2$ sample is found to harden by a few % on cooling from room temperature, which is the typical behavior induced by phonon hardening [120]. The flat temperature dependence in the orthorhombic state below T_s is ascribed to the multidomain effect outlined in the previous section and, in the following, we will therefore focus on data at $T > T_s$. We note that we find no evidence of a higher-temperature ($T > T_s$) nematic transition as proposed by Kasahara et al. [121] in any of our high-resolution shear modulus data. This is in agreement with previous high-resolution thermal-expansion measurements on both Co- and P-substituted $BaFe_2As_2$ [114,122], heat-capacity measurements in $BaFe_2(As_{1-x}P_x)_2$ [123], and stress-dependent measurements of phonon modes by Raman spectroscopy in $BaFe_2As_2$ [62], which also do not find evidence of an additional phase transition.

5.1. Doping and temperature dependence of the nematic susceptibility

Eq. (3) directly links C_{66} to the nematic susceptibility χ_φ under the assumption that the structural transition is induced by bilinear coupling to a nematic order parameter, Eq. (1). In real systems, the bare elastic constant $C_{66,0}$ is slightly temperature dependent because of phonon anharmonicity and typically hardens by a few % upon cooling between room temperature and zero temperature [120]. In order to remove this background contribution and to connect with the Young modulus, we make the approximation

$$\frac{Y_{[110]}}{Y_0} \approx \frac{C_{66}}{C_{66,0}} \tag{10}$$

Here, Y_0 is the non-critical contribution to $Y_{[110]}$ for which we use the data from a 33% Co substituted sample and further assume that it is independent of doping [114]. Additional details can be found in [23,24]. Assuming that the structural

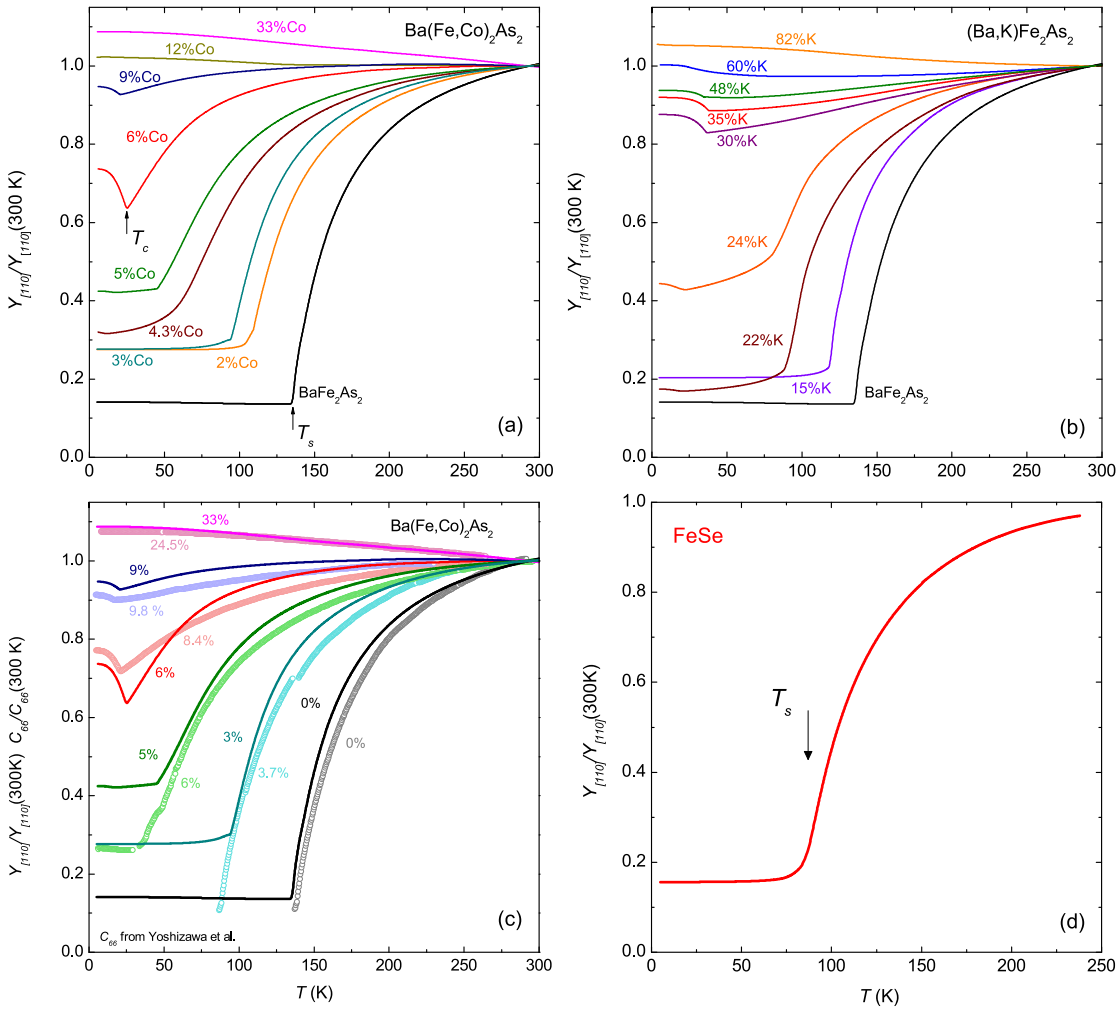

Fig. 4. Young's modulus along the tetragonal [110] direction $Y_{[110]}$ of (a) $Ba(Fe_{1-x}Co_x)_2As_2$ and (b) $Ba_{1-x}K_xFe_2As_2$ for a wide doping range, measured using the static three-point bending in a capacitance dilatometer described in Section 3. The data for $T < T_s$ are dominated by the effect of structural twins, similar to the low-stress measurements of Fig. 3. (c) Young's modulus $Y_{[110]}$ (lines) and shear modulus C_{66} (symbols, from Ref. [101]) for Co-doped $BaFe_2As_2$. Both quantities are normalized at room temperature. The indicated Co content is taken from Ref. [101] and samples with similar transition temperature are compared. All essential features, namely the strong softening of $Y_{[110]}$ on cooling towards T_s, and the marked hardening below T_c for moderately overdoped samples, are reproduced in Young's modulus data. Those curves show, however, a slightly stronger curvature than C_{66}, presumably because of the contributions from the other elastic constants (see Eq. (9)). (d) Young's modulus $Y_{[110]}$ of single crystalline FeSe, which shows very similar softening on cooling towards T_s.

transition of FeSe is also induced by bilinear coupling between a nematic order parameter and the lattice, φ is inferred from Young's modulus data of FeSe in the same way, assuming similar Y_0 [27]. The obtained bare nematic susceptibility χ_φ is plotted in Fig. 5(a, b, e) in units of $\lambda^2/C_{66,0}$. Note that the nematic susceptibility renormalized by the coupling to the lattice can be inferred easily using $\left(\lambda^2\tilde{\chi}_\varphi/C_{66,0}\right)^{-1} = \left(\lambda^2\chi_\varphi/C_{66,0}\right)^{-1} - 1$. χ_φ increases strongly with decreasing temperature for all but the most strongly overdoped $BaFe_2As_2$ samples. Interestingly, FeSe is found to resemble closely underdoped $BaFe_2As_2$.

The inverse $(\chi_\varphi)^{-1}$, plotted in Fig. 5(c, d, f), evidences a mean-field-type temperature dependence $\chi_\varphi = 1/(a(T - T_0))$ for $Ba(Fe_{1-x}Co_2)_2As_2$ up to $x = 0.09$, in agreement with Ref. [101], for $Ba_{1-x}K_xFe_2As_2$ up to $x = 0.24$ and for FeSe. However, and somewhat surprisingly, $Y_{[110]}$ does not follow a Curie–Weiss law in the higher doped $Ba_{1-x}K_xFe_2As_2$ samples in which the structural transition is suppressed. Instead, the temperature dependence is found to be less "critical" and $Y_{[110]}$ displays a clear inflection point. The detailed doping and temperature dependence of χ_φ is presented in Fig. 6. The color map of χ_φ in Fig. 6(a) shows that the nematic susceptibility is enhanced fairly symmetrically over most of the superconducting domes of both $Ba(Fe_{1-x}Co_x)_2As_2$ and $Ba_{1-x}K_xFe_2As_2$, suggesting its possible role in promoting superconductivity [23]. To describe the temperature dependence of χ_φ for different doping levels, we consider two parameters. First, we define T^* as either the inflection point of $\chi_\varphi(T)$ or its maximum value, whichever is greater. T^* is thus a lower limit for the validity of a Curie–Weiss law. Second, deviations from the Curie–Weiss law are ascribed to a temperature dependence of the parameter

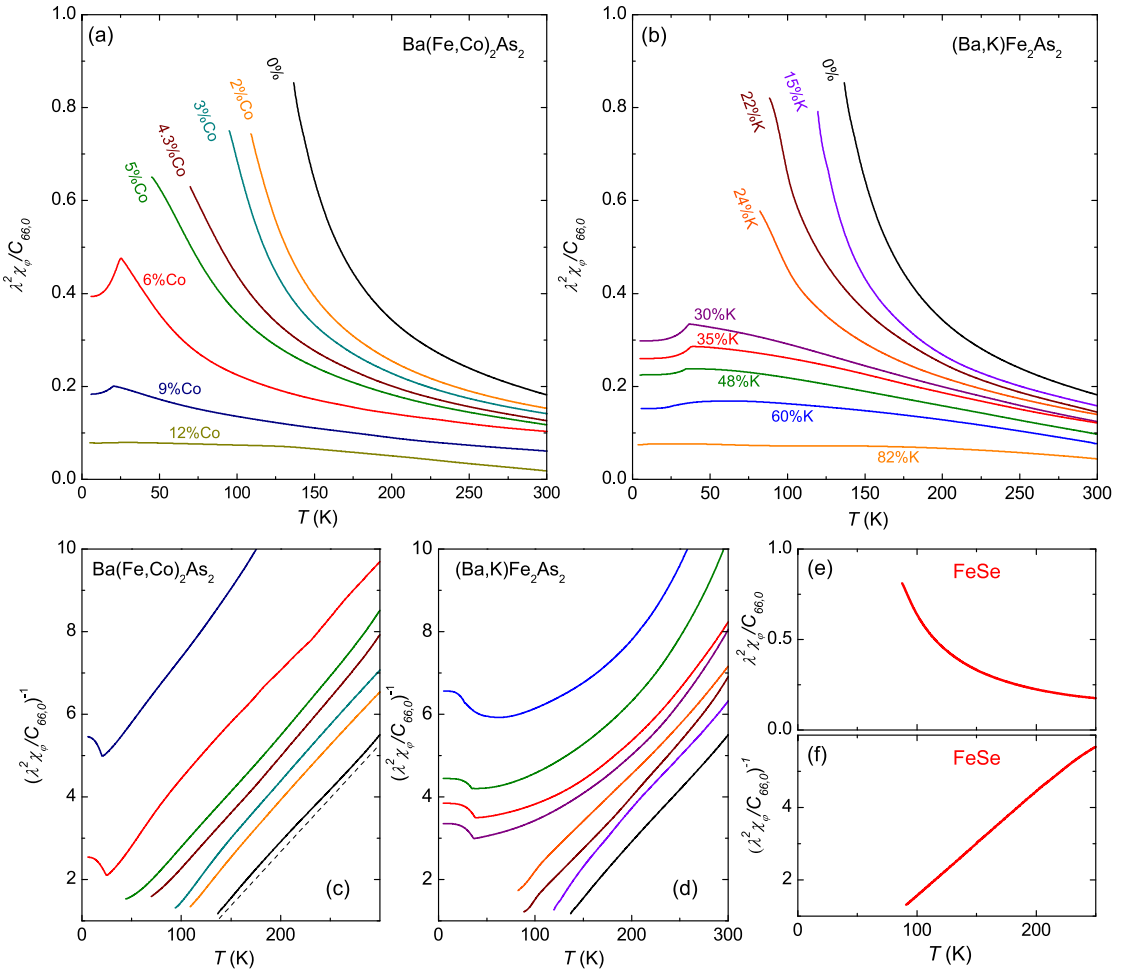

Fig. 5. Nematic susceptibility χ_φ in units of $C_{66,0}/\lambda^2$ of (a) $Ba(Fe_{1-x}Co_x)_2As_2$ and (b) $Ba_{1-x}K_xFe_2As_2$ obtained from the data in Fig. 4. For a second order structural phase transition $C_{66,0}/\lambda^2$ should reach 1 at T_s and it is unclear why the experimental data do not reach this value. (c), (d) show the inverse $\left(\lambda^2\chi_\varphi/C_{66,0}\right)^{-1}$ revealing a Curie–Weiss-like temperature dependence of the nematic susceptibility for all samples except $Ba_{1-x}K_xFe_2As_2$ with $\geq 30\%$ K content. The dashed straight line in (c) is a guide to the eye. (e) and (f) show similar data for FeSe, which resemble closely underdoped $BaFe_2As_2$.

T_0, whose value at fixed temperatures is plotted in Fig. 6(b). T^* reaches near zero temperature around optimal doping, which is consistent with a quantum critical scenario [101] only in the $Ba(Fe_{1-x}Co_x)_2As_2$ system. In contrast, T^* does not go below ~ 75 K in $Ba_{1-x}K_xFe_2As_2$. The findings suggest a first-order transition between different ground states preempting a quantum critical point in $Ba_{1-x}K_xFe_2As_2$, in particular the step-like change of T_0 between 24% and 30% K content (Fig. 6(b)). Interestingly, a new, C_4-symmetric, magnetic phase was subsequently found to emerge in between these two doping levels [98].

In Ref. [124], $C_{66}(T)$ was calculated including vertex corrections and was found not to follow the mean-field-type Curie–Weiss law. The data in Figs. 4 and 5 can be well described in this approach, for which the change of behavior of $Ba_{1-x}K_xFe_2As_2$ between 24% and 30% K content would be a consequence of a simple change of parameters as might be due to, e.g., a Lifshitz transition [124]. Finally, it is notable that the Curie constant $\lambda^2/aC_{66,0} = T_s^{CW} - T_0 \approx 30$–$40$ K, which is the characteristic energy of the electron–lattice coupling, is found to be nearly doping independent up to 9% Co content and 24% K content, the compositions for which it can be evaluated. Note that a value of ∼50–60 K is found for same parameter by evaluating C_{66} ultrasound data in the $Ba(Fe_{1-x}Co_x)_2As_2$ system [101]. This value is comparable but slightly larger than our result, and reflects the lower curvature of the C_{66} with respect to the $Y_{[110]}$ data in Fig. 4(c).

5.2. Young's modulus around T_c

Besides the softening due to the nematic transition, the high resolution of our three-point-bending experiment can also be used to study the behavior at and below the superconducting transition. In Fig. 7, we show our Young's modulus data for Co- and K-doped $BaFe_2As_2$ as well as for FeSe around T_c in detail. For most samples, a pronounced hardening of $Y_{[110]}$ below T_c is observed, while for some compositions of strongly overdoped $BaFe_2As_2$ and FeSe a small step-like softening of

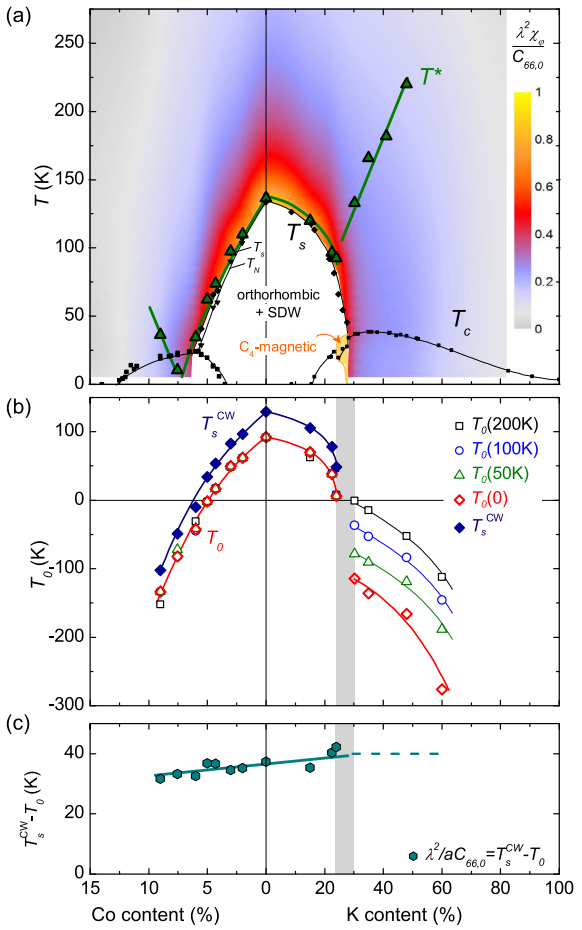

Fig. 6. (a) Nematic susceptibility as a color-coded map in the composition-temperature phase diagram of $Ba(Fe_{1-x}Co_x)_2As_2$ and $Ba_{1-x}K_xFe_2As_2$. Green triangles show the inflection point of $\chi_\varphi(T)$ as a lower limit for the validity of the Curie–Weiss law $\lambda^2\chi_\varphi/C_{66,0} = \frac{\lambda^2/aC_{66,0}}{T-T_0}$ (see text). (b) Weiss temperature T_0 and temperature at which C_{66} extrapolates to zero, T_s^{CW}. When the data deviate from the simple Curie–Weiss law, as for samples with ≥ 30 % K content, this deviation is ascribed to a temperature-dependent T_0 and T_0 (extrapolated) at various temperatures is reported. The dashed area indicates the doping range, in which an abrupt change suggests a first-order transition between different ground states. (c) Curie constant $\lambda^2/aC_{66,0} = T_s^{CW} - T_0$. The dashed line shows the extrapolation for the region where the data do not follow the Curie–Weiss law, used to obtain $T_0(T)$ in (b).

$Y_{[110]}$ at T_c is also visible. A hardening of the elastic shear modulus C_{66} below T_c was reported previously in overdoped $Ba(Fe_{1-x}Co_x)_2As_2$ [21,101]. As explained below, this effect is unusual in its sign, shape and magnitude for the effect of superconductivity on an elastic modulus.

The usual thermodynamic signature of a second-order phase transition in Young's modulus or any other elastic modulus is a small sudden softening upon cooling, which is related to the strain/stress dependence of T_c. Such a discontinuity is expected because the Young modulus Y_i is the inverse of a component of the elastic compliance S_{ii}, which, in turn, is a second derivative of the free energy. An Ehrenfest-type relation relates the size of this discontinuity at T_c, ΔY_i, to the uniaxial-pressure derivative dT_c/dp_i,

$$\Delta Y_i = -Y_i^2 \left(\frac{dT_c}{dp_i}\right)^2 \Delta C_p/T_c \tag{11}$$

Here, $\Delta C_p > 0$ is the specific-heat discontinuity at T_c and i stands for the direction. Note that necessarily $\Delta Y_i < 0$, i.e. Y_i shows a step-like decrease on cooling through the transition. Also, the shear modulus C_{66} alone is not expected to have such discontinuity, because the first derivative of T_c with respect to a shear deformation necessarily vanishes [125]. Hence, any discontinuity in the Young modulus arises from the contribution of the longitudinal elastic constants (the 'γ' in Eq. (9)) and $\Delta Y_{[110]}/Y_{[110]}^2 = \Delta Y_{[100]}/Y_{[100]}^2$. It has been pointed out in Ref. [126] that for an exotic superconducting state that mixes nematic fluctuations and s- and d-wave superconductivity and breaks tetragonal symmetry, even C_{66} can have a discontinuity at T_c. Such a state might occur in overdoped $Ba_{1-x}K_xFe_2As_2$ [126]; however, the Young modulus is not an

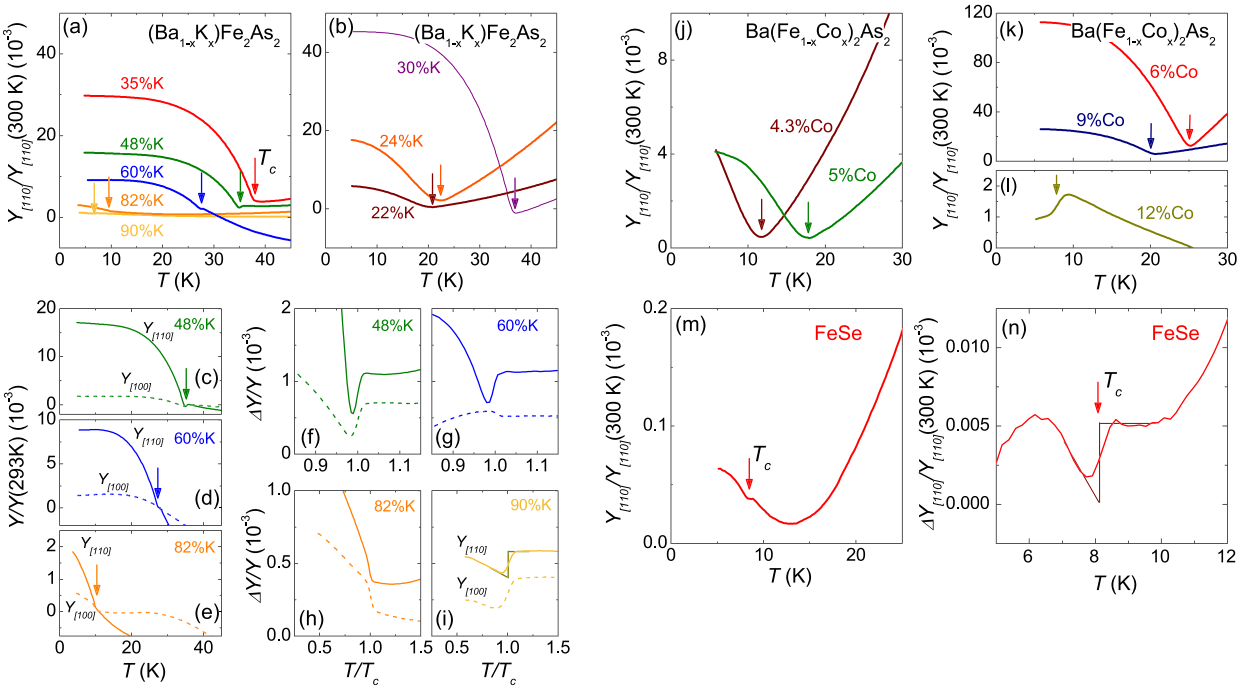

Fig. 7. Enlarged view of the low-temperature Young modulus $Y_{[110]}$ of (a) overdoped and (b) underdoped $Ba_{1-x}K_xFe_2As_2$, showing a pronounced hardening below T_c up to 82% K content. (c)–(e) Low-temperature Young's modulus along [110], $Y_{[110]}$, (solid line) and along [100], $Y_{[100]}$, (dashed line) of overdoped $Ba_{1-x}K_xFe_2As_2$, showing that the hardening occurs only in the [110] direction. (f)–(i) Enlarged view of the data close to T_c showing an additional small step-like anomaly ΔY_i at T_c. A linear background has been subtracted from the data. (j)–(l) Same as in (a), (b) for $Ba(Fe_{1-x}Co_x)_2As_2$. (m) Enlarged view of the low-temperature Young modulus of FeSe. (f) Even further enlarged view of the Young modulus of FeSe around T_c, with a linear background subtracted. Vertical arrows mark T_c in all panels. Data in (a)–(e) and (j)–(m) have been shifted vertically for better comparison. Lines in (i), (n) indicate an ideal second-order phase transition.

ideal probe to search for this effect, since it also contains the contribution from longitudinal elastic constants, as mentioned above.

Fig. 7 presents our Young modulus data in the vicinity of T_c in detail. The hardening of $Y_{[110]}$ below T_c is resolved for $Ba_{1-x}K_xFe_2As_2$ up to 82% K content and $Ba(Fe_{1-x}Co_x)_2As_2$ up to 9% Co content (panels (a), (b), (j), (k)). Note that the effect is even observed for underdoped samples, when T_c lies within the orthorhombic state and Young's modulus is actually dominated by the effect of structural twins (see Section 4). As detailed in Ref. [21], a hardening of the shear modulus C_{66} shows that nematic fluctuations, which decrease C_{66}, are weakened in the superconducting state. Its observation up to 82% K content indicates the presence of such nematic fluctuations over a large part of the superconducting dome in the phase diagram of $Ba_{1-x}K_xFe_2As_2$, although the degree of hardening strongly decreases with doping. Since this kind of response of $Y_{[110]}$ to superconductivity derives from the contribution of the shear modulus C_{66}, it should not be present in Young's modulus along [100], $Y_{[100]}$, which does not contain any contribution from C_{66}. Consistently, panels (c), (d), (e) show that such a hardening is not present in $Y_{[100]}$ of overdoped $Ba_{1-x}K_xFe_2As_2$, and very small effects may be due to sample misalignment.

In FeSe, such a hardening of $Y_{[110]}$ setting in abruptly at T_c is not observed, which can be taken as a sign that orthorhombic distortion and superconductivity do not compete in the same way as in doped $BaFe_2As_2$ in this material [70,27]. However, there is a very slight hardening of $Y_{[110]}$ (two orders of magnitude smaller than for similar $Ba(Fe_{1-x}Co_x)_2As_2$ samples) with an onset well above T_c, which correlates with an anomalous uniaxial thermal expansion seen previously [70]. The origin of this effect is unclear at this point and it may possibly be a consequence of the presence of very small Fermi energies in the system [76,75,127,128]. For some compositions of strongly overdoped $Ba_{1-x}K_xFe_2As_2$ (Fig. 7(f, g, i)), for $Ba(Fe_{0.88}Co_{0.12})_2As_2$ (Fig. 7(l)), and for FeSe (Fig. 7(n)), we can also resolve the small step-like softening of $Y_{[110]}$ and $Y_{[100]}$ expected from thermodynamics (Eq. 11). Using additional specific-heat data [129,130,27], the pressure-derivative of T_c is calculated via Eq. (11) and shown in Table 1. The uniaxial pressure derivative dT_c/dp_i can also be calculated by using uniaxial thermal expansion and specific heat via a similar Ehrenfest relation $dT_c/dp_i = V_m\Delta\alpha_i/\Delta(C_p/T)$. As shown in Table 1, the pressure derivatives derived from evaluating either Young's modulus or the thermal-expansion [70,98,131] data agree quite well. It is unclear why we do not resolve this step-like softening of the Young modulus either in the $Ba_{0.18}K_{0.82}Fe_2As_2$ sample or in the $Y_{[100]}$ of the $Ba_{0.4}K_{0.6}Fe_2As_2$ sample. These, instead, seem to show a step-like hardening that cannot be explained with Eq. (11).

Table 1
Uniaxial in-plane pressure derivative $|dT_c/dp_a|$ (sixth column), inferred using the Ehrenfest relation, Eq. (11), from the discontinuity of the Young modulus at T_c (third column, Fig. 7) and the specific heat (fifth column). A high-temperature Young modulus $Y_i(300\ \mathrm{K}) = 80$ GPa has been assumed in all cases. The obtained value should be the same for the two in-plane directions $i = [110]$ and $i = [100]$. For comparison, the last column shows dT_c/dp_a inferred from uniaxial thermal-expansion and specific heat data. The sign of dT_c/dp_a can only be obtained from thermal expansion.

	i	$\frac{\Delta Y_i}{Y_i(300\ \mathrm{K})}$ (10^{-3})	$\frac{Y_i(T_c)}{Y_i(300\ \mathrm{K})}$	$\Delta C_p/T_c$ (mJ mol^{-1}K^{-2}) Refs. [129,70,132]	$\left\|\frac{dT_c}{dp_a}\right\|$ (K/GPa) Eq. (11)	$\frac{dT_c}{dp_a}$ (K/GPa) Refs. [114,70,27]
$Ba_{0.52}K_{0.48}Fe_2As_2$	[100]	−0.62	1.03	126	1.9	−2.3
$Ba_{0.52}K_{0.48}Fe_2As_2$	[110]	−1	0.92	126	2.7	−2.3
$Ba_{0.40}K_{0.60}Fe_2As_2$	[110]	−0.73	0.99	96	2.5	−2.5
$Ba_{0.10}K_{0.90}Fe_2As_2$	[100]	−0.25	1.07	50	1.8	−2.2
$Ba_{0.10}K_{0.90}Fe_2As_2$	[110]	−0.18	1.05	126	1.6	−2.2
$Ba(Fe_{0.88}Co_{0.12})_2As_2$	[110]	−0.8	1.02	9	8	≈12
FeSe	[110]	−0.0051	0.16	5.6	3.2	3

6. Different probes of the nematic susceptibility

Quite generally, the nematic susceptibility can be probed by measuring the sensitivity of the electronic anisotropy of various quantities to uniaxial stress or strain. The most detailed data have been obtained using strain-dependent resistivity [25,133,45,134]. The electronic Raman response in different symmetry channels provides another probe [63] without actually having to apply any stress or strain to the crystal. In this section, we briefly review these studies and compare them to the results of our shear-modulus measurements. We note that there are also other probes that were used to obtain the nematic susceptibility, e.g., stress-dependent measurements of the optical reflectivity [42,43], and these agree in general well with our elastic data.

6.1. Elastoresistivity

The elastoresistivity is defined as the resistance change induced by sample deformation (strain) and is closely related to the piezoresistivity, which is the resistance change due to stresses acting on the sample [133]. Since the in-plane resistance anisotropy can be taken as a proxy for the nematic order parameter in the iron-based systems, there is an elastoresistivity coefficient, namely m_{66}, which is directly linked to the nematic susceptibility. In Refs. [25,133,134], the in-plane resistivity anisotropy N of iron-based materials was measured as a function of strain ε_6, externally applied to the sample via a piezo stack. Making use of the bilinear coupling λ between nematic order parameter and shear deformation, one obtains from Eq. (1), $2m_{66} = dN/d\varepsilon_6 \propto d\varphi/d\varepsilon_6 = \lambda\chi_\varphi$ [25,134]. Note that by measuring the strain instead of the stress dependence of N the elastic properties of the material are "short-circuited" and, therefore, the bare electronic nematic susceptibility χ_φ, and not the renormalized $\tilde{\chi}_\varphi$ is expected to be measured [25]. The proportionality constant between N and φ is related to the details of the Fermi surface and electronic scattering and can, in principle, be temperature, as well as doping dependent. It was shown that m_{66} follows a Curie–Weiss law $\sim 1/(T - T_0)$ in $BaFe_2(As_{0.7}P_{0.3})_2$ [134], which advocates that this proportionality constant is only very weakly temperature dependent. Further, Ni- and Co-doped samples with the same T_s were compared [45]. Ni doping induces larger scattering (lower RRR) than Co doping; however, it was found that the elastoresistivity m_{66} is independent of this kind of disorder for $T > T_s$ [45].

As mentioned previously, the structural transition may, in principle, arise either from a divergence of χ_φ, as in an electronically-driven transition (as assumed here), or from vanishing $C_{66,0}$, as in a bare lattice instability. The quantity obtained by the shear modulus measurements, $\lambda^2\chi_\varphi/C_{66,0}$ diverges in both cases. Notably, the elastoresistivity $m_{66} \propto \lambda\chi_\varphi$ is independent of the bare shear modulus $C_{66,0}$. If the lattice caused the transition, then $\lambda^2\chi_\varphi/C_{66,0}$ would diverge, but $\lambda\chi_\varphi$ would show no strong temperature dependence. The experiment by Chu et al. [25] showed that, however, $\lambda\chi_\varphi$ also diverges, which was taken as a proof that φ drives the transition and that the lattice distortion is just a consequence of the bilinear coupling to φ [25].

Elastoresistivity measurements of the optimally doped compounds $BaFe_2(As_{0.7}P_{0.3})_2$, $Ba_{0.6}K_{0.4}Fe_2As_2$, $Ba(Fe_{0.93}Ni_{0.07})_2As_2$, $Ba(Fe_{0.955}Ni_{0.045})_2As_2$, $Fe(Te_{0.6}Se_{0.4})$ [134] as well as of FeSe [74] show that the elastoresistivity coefficient m_{66} diverges following an approximate Curie–Weiss law in all of these systems, though deviations below ~ 100 K are sometimes observed. We note that the quantity $\lambda^2\chi_\varphi/C_{66,0}$ obtained from the shear modulus is normalized such that it reaches (ideally) the value 1 at the phase transition, equivalent to a vanishing C_{66}. In contrast, the elastoresistivity is not normalized and the value of m_{66} is indeed found to be somewhat doping dependent. It seems, e.g., to peak around optimal doping in $Ba(Fe_{1-x}Co_x)_2As_2$, which was suggested to be due to enhanced fluctuations near a quantum critical point [134]. However, m_{66} still has a similar magnitude in all of the studied iron-based systems, although its sign depends on the particular system.

6.2. Electronic Raman scattering

Electronic Raman scattering of $Ba(Fe_{1-x}Co_x)_2As_2$ [135,63] finds an enhancement of the Raman response in the B_{2g} symmetry channel (which is the symmetry that corresponds to the orthorhombic distortion) with respect to the B_{1g}

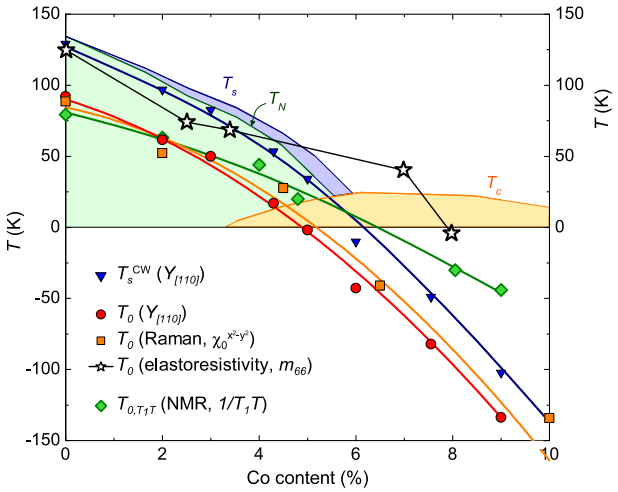

Fig. 8. Weiss temperature T_0 obtained by fitting the nematic susceptibility as determined by Young's modulus $Y_{[110]}$ [23] (red circles), electronic Raman scattering [63] (orange squares) and elastoresistivity m_{66} [134] (black open stars) measurements in $Ba(Fe_{1-x}Co_x)_2As_2$. Also given is the Weiss temperature T_{0,T_1T} of the spin–lattice relaxation rate divided by temperature $1/T_1T$ in nuclear magnetic resonance [139,140] (green diamonds). Lines are a guide to the eye. The phase transition temperatures T_s, T_N and T_c [12] are indicated by thin colored lines and areas. T_s^{CW}, the temperature at which C_{66} extrapolates to zero, is indicated by blue triangles.

symmetry channel. Using Kramer's Kronig relations, the static nematic charge susceptibility $\chi_0^{x^2-y^2}$ was extracted from the data. $\chi_0^{x^2-y^2}$ of $Ba(Fe_{1-x}Co_x)_2As_2$ was found to increase on approaching the structural transition, though it does not diverge at T_s. It, indeed, follows a Curie–Weiss law for a wide doping range [63]. Recently, Raman scattering data and $\chi_0^{x^2-y^2}$ was also reported for FeSe and $Ba_{1-x}K_xAs_2As_2$ [136]. While $\chi_0^{x^2-y^2}$ of FeSe and underdoped $Ba_{1-x}K_xAs_2As_2$ shows the same Curie–Weiss-like divergence, deviations from the Curie–Weiss law were observed for close-to-optimally-doped $Ba_{1-x}K_xAs_2As_2$ samples.

In Ref. [124], both the shear modulus and the Raman susceptibility have been calculated in the five orbital models, including vertex corrections. It was noted that the Raman susceptibility is less singular than the shear modulus because the photons cannot couple to the acoustic lattice vibrations due to the mismatch of their wavelength for the same frequency [124]. In this sense, the charge nematic susceptibility in Raman scattering should be similar to the bare nematic susceptibility χ_φ and not $\tilde{\chi}_\varphi$, which is renormalized by coupling to the lattice [137]. Electronic Raman scattering as a probe of nematicity in iron-based systems is discussed in another contribution to this issue [138].

6.3. Comparison of shear modulus, elastoresistivity, and electronic Raman scattering

Among the above materials, the $Ba(Fe_{1-x}Co_x)_2As_2$ system has been studied most intensively. In this system, all three χ_φ (shear modulus, [23]), m_{66} (elastoresistivity [134]) and $\chi_0^{x^2-y^2}$ (electronic Raman scattering [63,135]) show a Curie–Weiss-like divergence. To make a quantitative comparison, we show in Fig. 8 the values of the Weiss temperature T_0 obtained by fitting these data to a Curie–Weiss law $\sim 1/(T - T_0)$. Note that in case of the m_{66} data, the low-temperature region, where m_{66} deviates somewhat from a Curie–Weiss law close to optimal doping, has been excluded from the fit [134]. We have also included T_{0,T_1T} obtained by fitting the spin–lattice relaxation rate divided by temperature $1/T_1T$ [139,140], since it also follows a Curie–Weiss temperature dependence [139]. $1/T_1T$ is related to the strength of the magnetic fluctuations, which the spin-nematic scenario explicitly links to the nematic susceptibility [3] (these data are discussed in the following Section 7). Also shown is T_s^{CW}, the temperature at which C_{66} extrapolates to zero, i.e., at which the structural transition would be expected (see Section 2). Why C_{66} does not quite reach zero and, hence, T_s^{CW} is lower than T_s is still an open question.

Intriguingly, T_0 as determined by electronic Raman scattering agrees quite well with the elastic data over the whole doping range, which supports that the charge nematic susceptibility $\chi_0^{x^2-y^2}$ of the Raman experiment is very closely related to the bare nematic susceptibility χ_φ obtained using the shear-modulus data. In contrast, the values of T_0 derived from the elastoresistivity data are considerably higher at all doping levels than those from the elastic and Raman data, which is unexpected within the Landau analysis of this quantity [25]. For this probe, T_0 appears even to cross the T_s line at around 5% Co content, which is also not expected in the simple Landau theory. This curiously high value of T_0 for the overdoped samples may partly be due to the exclusion of the low-temperature region from the fit of m_{66}. In this region, the divergence of m_{66} appears to be suppressed at lower temperature, which was attributed to disorder effects [134]. Such an effect appears to be either absent or much less pronounced in the Raman and Young's modulus data. Nevertheless, the

reason for this deviation of the T_0 values from m_{66} for underdoped as well as overdoped $Ba(Fe_{1-x}Co_x)_2As_2$ is unclear to us and deserves further attention.

For optimally doped $Ba_{1-x}K_xFe_2As_2$, the shear-modulus data (see Fig. 5) show strong deviations from a Curie–Weiss dependence of the nematic susceptibility, including a prominent inflection point. Interestingly, a very similar temperature dependence of the Raman susceptibility $\chi_0^{x^2-y^2}$ has also been observed in close to optimally doped $Ba_{1-x}K_xFe_2As_2$ [136]. On the other hand, the elastoresistivity coefficient m_{66} of optimally doped $Ba_{1-x}K_xFe_2As_2$ shows an approximate Curie–Weiss-like divergence [134]. Again, the origin of this difference is unclear to us. Finally, for FeSe, χ_φ [27], m_{66} [74] and $\chi_0^{x^2-y^2}$ [136,137] all show again the familiar Curie–Weiss temperature dependence $\sim 1/(T-T_0)$.

7. Magnetic correlations as the origin of nematicity?

In the itinerant spin-nematic scenario of Refs. [20,21,3], magnetic correlations are at the origin of nematicity and, ultimately, of the structural phase transition. Hence, it should be possible to derive the elastic properties of iron-based materials from their magnetic properties. Indeed, a scaling relation between $1/T_1T$, as a measure of the strength of spin fluctuations, and the shear modulus C_{66} has been derived in this theory, which provides a useful test of the scenario [26]. Here, we briefly review the derivation of this scaling between spin–lattice relaxation rate $1/T_1$ and C_{66} and then we check the scaling using experimental data in three different iron-based systems.

7.1. Scaling relation between T_1T and C_{66}

An expression for the nematic susceptibility in terms of the dynamic spin susceptibility χ is calculated in Ref. [21] as

$$\left(\chi_\varphi\right)^{-1} = \frac{1}{\sum_q \chi^2(q)} - g_0 \tag{12}$$

(see also Ref. [3]), where g_0 is a "bare" nematic coupling constant. χ_φ is renormalized by bilinear coupling with the elastic system (as in Eq. (1)) to

$$\left(\tilde{\chi}_\varphi\right)^{-1} = \frac{1}{\sum_q \chi^2(q)} - (g_0 + \lambda^2/C_{66,0}) \tag{13}$$

where $g = g_0 + \lambda^2/C_{66,0}$ is the renormalized nematic coupling and the crucial parameter of the theory. $q = (\mathbf{q}, \omega)$ stands for the momentum and frequency dependence. The magnetic transition occurs when $\sum_q \chi^2(q)$ diverges, but if $g > 0$ it is sufficient for $\sum_q^2 \chi(q)$ to reach a finite threshold value (i.e. $1/g$) to cause a divergence of $\tilde{\chi}_\varphi$ and induce the nematic/structural transition. This is the explanation why T_s can be higher than T_N in this scenario, even though both transitions are driven by magnetic fluctuations. The spin susceptibility χ can be accessed by the spin–lattice relaxation rate divided by temperature, as measured in NMR experiments,

$$\frac{1}{T_1T} = \gamma_g^2 \lim_{\omega\to\omega_0} \sum_{\mathbf{q}} F^2(\mathbf{q}) \frac{\mathrm{Im}\,\chi(\mathbf{q},\omega)}{\omega} \tag{14}$$

Here, ω_0 is the NMR frequency, which is considered to be very small and $F(\mathbf{q})$ is a momentum-dependent form factor that peaks at the ordering wave vectors Q_1 and Q_2 when the magnetic field is applied parallel to the *ab* plane [141]. As shown in detail in Ref. [26], $1/T_1T$ measured with the magnetic field in the *ab* plane is proportional to $\sum_q \chi^2(q)$ under certain approximations (assuming overdamped dynamics $(\chi(\mathbf{q},\omega))^{-1} = (\chi(\mathbf{q}))^{-1} - i\omega\Gamma$, vicinity of a finite-temperature critical point so that $\sum_q \chi^2(q)$ can be replaced by $T_0\sum_{\mathbf{q}} \chi^2(\mathbf{q})$, and the replacement of the form factor $F(\mathbf{q}) \to F(Q)$ because of the direction of the applied field). Using this proportionality, one can express χ_φ and, with the help of Eq. (3), C_{66} in terms of T_1,

$$\frac{C_{66}}{C_{66,0}} = \frac{1}{1 + (aT_1T - b)^{-1}} \tag{15}$$

with the two parameters a and b [26]. The parameter b is particularly interesting, since it provides a measure of the nematic coupling strength $b = \frac{C_{66,0}}{\lambda^2} g$, while a contains the strength of the hyperfine interaction, see Ref. [26].

7.2. Test of the $1/T_1T$–C_{66} scaling relation in Co- and K-doped $BaFe_2As_2$

Fig. 9(a) shows $1/T_1T$ data of $Ba(Fe_{1-x}Co_x)_2As_2$ from Refs. [139,140], measured under an in-plane magnetic field and Fig. 10(a) shows the equivalent data for $Ba_{1-x}K_xFe_2As_2$ from Ref. [142]. We first discuss the $Ba(Fe_{1-x}Co_x)_2As_2$ system. Eq. (15) considers only the fluctuations around the AFM wave vector Q, which are referred to as "interband" contribution in Ref. [139]. The non-critical "intraband" contribution has to be subtracted from the data as a background. Following Ref. [139], this is achieved by subtracting the data for the strongly overdoped $Ba(Fe_{0.86}Co_{0.14})_2As_2$, modeled as $(1/T_1T)_{\mathrm{intra}} = 0.11\ \mathrm{K^{-1}s^{-1}} + 0.63\ \mathrm{K^{-1}s^{-1}} \exp(-450\ \mathrm{K}/T)$ (black line in Fig. 9(a)). The obtained $(1/T_1T)_{\mathrm{inter}}$ can be scaled onto the elastic data according to Eq. (15), and the result is shown in Fig. 9(b), where the scaling parameters a and b are given in the inset.

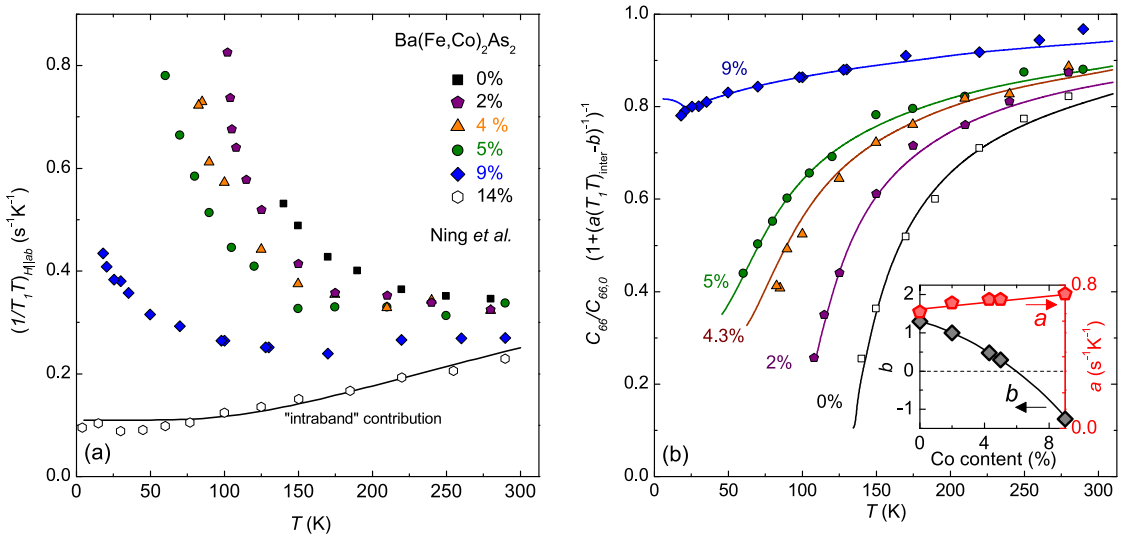

Fig. 9. (a) Spin–lattice relaxation rate divided by temperature $1/T_1T$ of $Ba(Fe_{1-x}Co_x)_2As_2$ with magnetic field $H||ab$, from Refs. [139,140]. The data for the 14% doped sample are taken as a background (black line). (b) Scaling analysis of the shear modulus $C_{66}/C_{66,0}$ and spin–lattice relaxation rate. The lines are obtained from three-point bending, while the symbols show the data of (a), scaled according to Eq. (15) after subtraction of the background. The scaling parameters are reported in the inset.

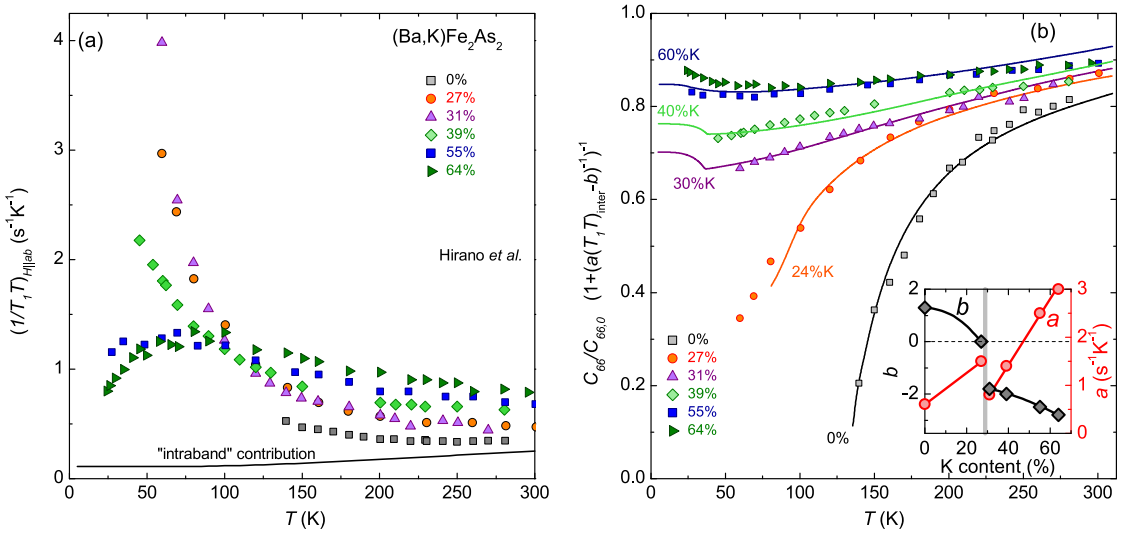

Fig. 10. Same as Fig. 9 but for $Ba_{1-x}K_xFe_2As_2$. NMR data with field $H||ab$ are taken from Ref. [142]. The vertical line in the inset marks the K content at which the structural transition is suppressed in a first-order-like fashion and the temperature dependence of the nematic susceptibility changes abruptly (see Fig. 6).

The scaling works very well for all Co substitution levels, supporting a magnetic origin of the shear-modulus softening [26]. Alternatively, a phenomenological linear scaling between C_{66} and $1/T_1T$ was proposed in Ref. [143], which, however, does not work as well. Note that the parameter b is proportional to the difference between the Weiss temperatures T_0 and T_{0,T_1T} of the nematic susceptibility χ_φ and $1/T_1T$, respectively, which are shown in Fig. 8. Interestingly, T_0 and T_{0,T_1T} cross and b changes sign around the critical composition where the structural transition is suppressed. However, the assumption of a finite-temperature critical point used to derive the scaling relation is not strictly valid in this doping region and, hence, this sign change of b might be an artefact. However, if b, or, equivalently, g really becomes negative for overdoped $Ba(Fe_{1-x}Co_x)_2As_2$, it would indicate that a non-nematic, C_4-symmetric magnetic state is preferred over the stripe-type one. Such a C_4-symmetric magnetic phase is, indeed, found to be induced by Na or K substitution in $BaFe_2As_2$ very close to the critical point [92,98].

We note that a similar scaling attempt in Ref. [63], between the nematic charge susceptibility $\chi_0^{x^2-y^2}$ measured using electronic Raman scattering, and the elastic modulus failed. Here, the authors equated the $\chi_0^{x^2-y^2}$ with the renormalized

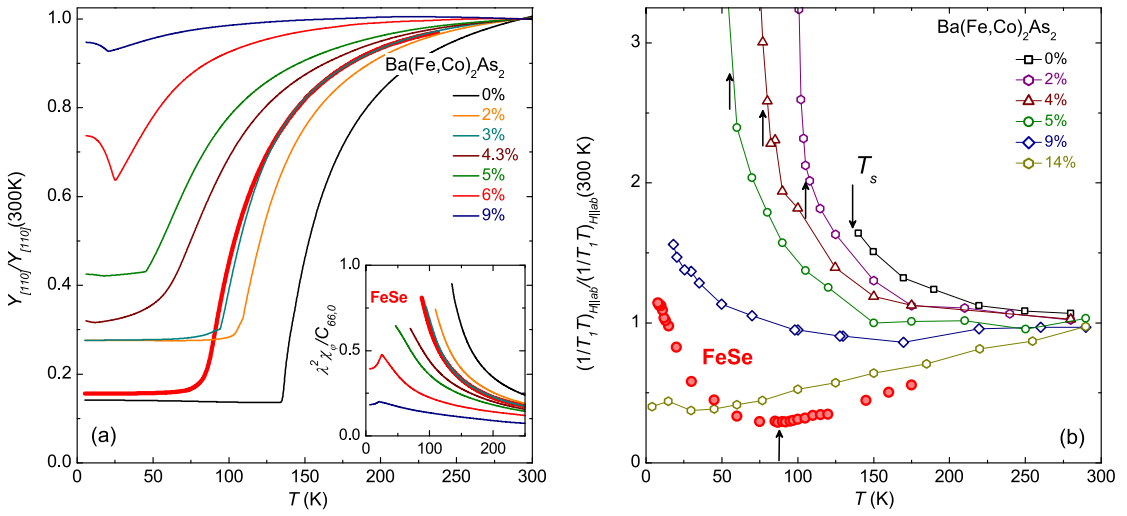

Fig. 11. (a) Young's modulus $Y_{[110]}$ of FeSe, superimposed on the data for $Ba(Fe_{1-x}Co_x)_2As_2$. FeSe fits very well in the series. The inset shows the nematic susceptibility (see Eq. (3)). (b) $1/T_1T$ normalized by its (extrapolated) value at room temperature of FeSe and $Ba(Fe_{1-x}Co_x)_2As_2$ (data taken from Refs. [139,140]). Vertical arrows indicate T_s. While $1/T_1T$ of underdoped $Ba(Fe_{1-x}Co_x)_2As_2$ shows a strong increase on cooling towards T_s (and a steeper increase below), the data for FeSe only increase below T_s.

nematic susceptibility $\tilde{\chi}_\varphi$ so that the scaling takes the form $C_{66}/C_{66,0} = \left(1 + a\chi_0^{x^2-y^2}\right)^{-1}$ (deduced using Eq. (4)) with a single parameter a. However, when assuming that $\chi_0^{x^2-y^2}$ reflects the bare nematic susceptibility χ_φ [124,137], the form of the scaling should rather be identical to Eq. (15), which does work well also for the Raman data of $Ba(Fe_{1-x}Co_x)_2As_2$.

It is interesting to consider the scaling relation of $1/T_1T$ and C_{66} also in the $Ba_{1-x}K_xFe_2As_2$ system, for which both sets of data have been published [142,23], but scaling has not been attempted. The striking feature of this system is that both $1/T_1T$ and C_{66} do not follow a Curie–Weiss temperature dependence over the whole doping region. In particular, the nematic susceptibility as obtained from the shear modulus changes its temperature dependence abruptly between 24% and 30% K content. The NMR data from Ref. [142] show a similar change in the temperature dependence, however, occurring rather between 39% and 55%. In spite of the lack of a Curie–Weiss-like temperature dependence, it is remarkable that these data can be scaled quite well by Eq. (15) (Fig. 10). Tentatively, the same "intraband" background as for the $Ba(Fe_{1-x}Co_x)_2As_2$ system has been subtracted from the raw $1/T_1T$ data. The parameters a and b used in the scaling are shown in the inset of Fig. 10(b). There are several points of interest here. First, there is an abrupt change of both a and b at $\sim 25\%$ K content (marked by a vertical line), reflecting that the temperature dependence of C_{66} but not of T_1T changes abruptly. b is found to be close to zero just before the structural transition disappears, which is similar to the $Ba(Fe_{1-x}Co_x)_2As_2$ system. Beyond this concentration, b is negative indicating that the systems tends to a non-nematic magnetic order. Interestingly, the magnetic ground state of $Ba_{1-x}K_xFe_2As_2$ close to this K concentration seems, indeed, to be tetragonal and it would be fascinating to study NMR and shear modulus in detail for the respective substitution range. The parameter a also shows a strong dependence on the K content, while it is roughly independent of the Co content. Examining the scaling relation (Eq. (15)) shows that the parameter a renormalizes the magnitude of T_1T. The strong increase of a with doping reflects that the high-temperature values of $1/T_1T$ increase significantly with K content, which might reflect either a change in the hyperfine coupling (as would be correctly captured by a [26]) or a strongly doping-dependent background contribution. Note that $1/T_1T$ takes the largest value of all samples for pure KFe_2As_2 [142], even though it is supposedly far away from a magnetic instability.

7.3. Shear-modulus softening and magnetic fluctuations in FeSe

As described in the introduction, the iron-based superconductor FeSe is particularly interesting with respect to the relation between structure and magnetism. In particular, its large paramagnetic, orthorhombic (i.e. nematic) phase makes FeSe an interesting test case to study the origin of nematicity. As discernable from Figs. 4 and 5, $Y_{[110]}(T)$ of FeSe is very similar to that of underdoped $Ba(Fe_{1-x}Co_x)_2As_2$. In Fig. 11, we compare the two systems in detail. Curiously, the $Y_{[110]}$ and χ_φ values of FeSe are nearly identical to those of $Ba(Fe_{0.97}Co_{0.03})_2As_2$, which has a similar T_s [27]. The nearly identical temperature dependences indicate that the coupling $\lambda^2/aC_{66,0}$ has the same value in FeSe and in underdoped $Ba(Fe_{1-x}Co_x)_2As_2$, which is remarkable considering the differences between the two systems.

In light of this similarity of Young's modulus, it is somewhat surprising to find that the evidence for spin fluctuations from the spin–lattice relaxation data of FeSe is much less pronounced than in the $Ba(Fe_{1-x}Co_x)_2As_2$ system [69,27] (Fig. 11(b)). In contrast to underdoped $Ba(Fe_{1-x}Co_x)_2As_2$, $1/T_1T$ of FeSe shows an increase upon cooling only below T_s and, actually, decreases upon cooling from room temperature down to T_s. This drastic difference already suggests that

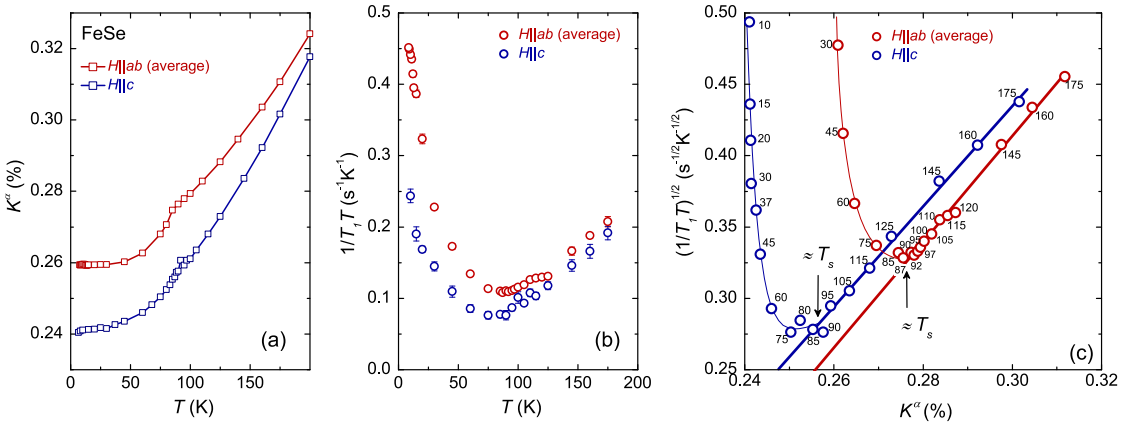

Fig. 12. (a) NMR spectral shift K^{α} and (b) spin–lattice relaxation rate divided by temperature $1/T_1T$ of single-crystalline FeSe with the field direction, α, in the *ab* plane (average of *a* and *b* axis in the orthorhombic state) and along the *c* axis. (c) shows a plot of $\sqrt{1/T_1T}$ vs. K^{α}, with the temperature as an implicit parameter indicated in units of K. The straight lines correspond to the Fermi-liquid-type Korringa relation (Eq. (16)), deviations from which show the emergence of a spin-fluctuation contribution. Such an additional contribution is evident only below T_s. The thin lines are a guide to the eye.

spin fluctuations may not be the origin of the diverging nematic susceptibility in FeSe. In order to exclude the possibility that a strongly temperature-dependent "intraband" background contribution hampers the determination of the relevant $(1/T_1T)_{\text{inter}}$ and, hence, the scaling analysis in FeSe, the NMR data have been analyzed in detail (see Fig. 12, [27]).

Fig. 12(a, b) show the spectral shift K^{α} and $1/T_1T$ of a collection of ~ 10 single crystals of FeSe, measured in a field of 9 T with the field direction α both in-plane and along the *c* axis. K^{α} has a pronounced temperature dependence, which can presumably be explained in a Fermi-liquid picture by the small Fermi energy [144] found in FeSe [76,75,127,128]. Since K and $1/T_1T$ are related by the Korringa relation for a Fermi liquid

$$\left(\frac{1}{T_1T}\right)_{\text{FL}} \propto K^2_{\text{spin}} \tag{16}$$

the temperature-dependent K^{α} will lead to a temperature-dependent $1/T_1T$. In order to isolate a possible contribution from spin fluctuations to $1/T_1T$, we tested Eq. (16) by plotting $\sqrt{1/T_1T}$ vs. K^{α} with temperature as an implicit parameter in Fig. 12(c). For both field directions, we found a linear relation between the two quantities, which shows that the Fermi-liquid Korringa relation is indeed satisfied down to T_s. Hence, this analysis shows the absence of any measurable spin-fluctuation contribution to $1/T_1T$ for $T > T_s$, in strong contrast to underdoped $BaFe_2As_2$. This means that such spin fluctuations cannot be the origin of the shear-modulus softening and, in consequence, the structural transition and nematicity in FeSe, and it is likely that the alternative orbital order drives the structural transition, as also suggested by ARPES studies [75,77]. A similar conclusion was reached by another NMR work by Baek et al. [73]. Curiously, the nematic susceptibility χ_{φ} of underdoped $Ba(Fe_{1-x}Co_x)_2As_2$ and FeSe is very similar, which may raise doubt on the magnetic origin of nematicity in $Ba(Fe_{1-x}Co_x)_2As_2$ as well. Finally, the NMR data on FeSe (Figs. 11 and 12) seem to suggest that the structural transition at T_s triggers the emergence of spin fluctuations. However, there is no such correlation under hydrostatic pressure, which enhances spin fluctuations [69], but suppresses T_s [82–84]. This result suggests an unusual relation between magnetic order and the structural transition in FeSe.

As we pointed out previously [27], inelastic neutron scattering experiments are needed to determine the nature of the magnetic fluctuations, and very recently the first of such experiments have been reported [78,79]. Surprisingly, these studies provide evidence of magnetic stripe-like $(\pi, 0)$ fluctuations in FeSe, similar to the 122 compounds. As in the other Fe-based materials, these magnetic fluctuations are found to occur already above T_s, in apparent contradiction to the NMR results. There is, however, evidence for a spin gap-like feature below ~ 2.5 meV in the neutron data already at 110 K [79], which can explain the absence of spin fluctuations in the NMR experiment, a probe that is sensitive only to the low-energy fluctuations. It is, hence, conceivable that those spin fluctuations can drive the structural transition of FeSe according to the spin-nematic scenario, without the scaling of shear modulus and NMR spin–lattice relaxation rate. However, the neutron experiments, which have been performed both on polycrystalline [78] and single-crystalline material [79], are not fully consistent with each other. In Ref. [78], the strength of the magnetic signal is temperature independent between 8 K and 104 K, whereas a strong temperature dependence is observed in Ref. [79]. These differences may also reflect differences in samples. The properties of FeSe samples depend strongly on the preparation technique. In particular, the samples prepared using a floating-zone technique used in Ref. [79] have undergone a phase transformation to the tetragonal, superconducting β-FeSe phase on cooling to room temperature. Such samples are not single phase [145] and do not show a clear tetragonal-to-orthorhombic structural transition in the resistivity [145]. The samples prepared by solid-state synthesis used in Ref. [78] show an unusual difference between their zero-field-cooled and field-cooled magnetic susceptibility values around T_s [78], which is different from the case of vapor-grown crystals [70]. Hence, the issue seems not fully resolved yet and more careful

neutron experiments on low-temperature vapor-grown crystals are still desirable. Finally, we mention that these puzzling features of FeSe, i.e. the nematic phase and the absence of magnetic order, have attracted the attention of theorists, and there are now several different proposed theoretical scenarios, including strong magnetic frustration [88], spin-quadropolar order [87], the formation of a quantum paramagnet [89], and charge–current density wave [91].

8. Summary and outlook

In this review we have compared the electronic nematic susceptibility of various iron-based superconducting materials derived from measurements of the shear modulus, the elastoresistivity, and the Raman response function. Particular emphasis has been put on our own studies of the Young modulus in $Ba(Fe_{1-x}Co_x)_2As_2$, $Ba_{1-x}K_xFe_2As_2$ and FeSe obtained via a three-point-bending technique in a capacitance dilatometer. In a Landau formalism, in which an electronic nematic order parameter drives the structural transition via bilinear coupling to the orthorhombic lattice distortion, the nematic susceptibility was obtained from the elastic data. The relation of this "thermodynamic" nematic susceptibility to spin- and orbital degrees of freedom is found to be intricate, and may be different for the different iron-based systems. Notably, the nematic susceptibility from the shear-modulus data seems to be closely related to the orbital nematic susceptibility from electronic Raman scattering in all the systems. On the other hand, the elastoresistivity behaves somewhat differently, in particular for optimally doped $Ba_{1-x}K_xFe_2As_2$. The excellent scaling of shear-modulus softening and spin–lattice relaxation rate $1/T_1$ in both $Ba(Fe_{1-x}Co_x)_2As_2$ and $Ba_{1-x}K_xFe_2As_2$ supports the notion that the structural transition is driven by magnetic fluctuations. FeSe seems to be an unusual case, in that there is no spin-fluctuation contribution to $1/T_1$ above the structural transition, even though the nematic susceptibility of FeSe and underdoped $Ba(Fe_{1-x}Co_x)_2As_2$ have a very similar temperature dependence, suggesting the importance of orbital degrees of freedom. However, very recent inelastic neutron scattering experiments suggest that spin fluctuations in FeSe are similar to those in the $BaFe_2As_2$-based systems. Further neutron studies on high-quality vapor-grown FeSe crystals are thus highly desirable.

The interrelationship of the various types of coupled order in iron-based systems—e.g., structural, orbital, magnetic and superconducting—has turned out to be a very rich field of study, and electronic nematicity has grown into one of the most intensively studied concepts in the field of iron-based superconductivity. The relationship between nematic fluctuations and superconductivity remains an interesting and open problem. Recently, evidence of a nematic resonance in the superconducting state was presented in Raman scattering experiments [146], suggesting a close link between nematic fluctuations and superconductivity. Further, the enhancement of superconductivity near a nematic quantum critical point has been investigated [147]. We believe that in order to obtain further insight into the microscopic origin of nematicity and its possible relation to superconductivity, the study of systems in which structural and magnetic transitions do not closely follow each other is particularly promising. In this context, FeSe and the magnetic C_4 phase in hole-doped $BaFe_2As_2$ have recently attracted a great deal of attention and may very well hold further surprises in the near future.

Acknowledgements

First, we would like to acknowledge Thomas Wolf for the excellent iron-based single crystals, without which our studies would not have been possible. We would like to especially thank W. Schranz and M. Reinecker for the opportunity to perform the dynamic three-point-bending experiments and for their hospitality in Vienna, and also Kenji Ishida and his group in Kyoto (T. Arai, T. Iye, T. Hattori) for the opportunity to make NMR measurements on FeSe and for their hospitality. We thank R.M. Fernandes and J. Schmalian for the very fruitful collaboration concerning the scaling of bending and NMR data. Further, we acknowledge fruitful and rewarding collaborations and discussions with F. Hardy, P. Burger, L. Wang, P. Schweiss, H. v. Löhneysen, U. Karahasanovic, M. Hoyer, P. Hlobil, A. Chubukov, S. Kasahara, T. Shibauchi, Y. Matsuda, I.R. Fisher, Y. Gallais, Y. Furukawa, A. Kreyssig, S.L. Bud'ko and P.C. Canfield. Part of this work was supported by the Japan–Germany Research Cooperative Program, KAKENHI from JSPS (Grant No. 25103712) and Project No. 56393598 from DAAD, and by the DFG through SPP 1458.

References

[1] E. Fradkin, S.A. Kivelson, M.J. Lawler, J.P. Eisenstein, A.P. Mackenzie, Nematic Fermi fluids in condensed matter physics, Annu. Rev. Condens. Matter Phys. 1 (2010) 153.
[2] R.M. Fernandes, A.V. Chubukov, J. Schmalian, What drives nematic order in iron-based superconductors?, Nat. Phys. 10 (2014) 97–104.
[3] R.M. Fernandes, J. Schmalian, Manifestations of nematic degrees of freedom in the magnetic, elastic, and superconducting properties of the iron pnictides, Supercond. Sci. Technol. 25 (2012) 084005.
[4] C. de la Cruz, Q. Huang, J.W. Lynn, J. Li, W. Ratcliff II, J.L. Zarestky, H.A. Mook, G.F. Chen, J.L. Luo, N.L. Wang, P. Dai, Magnetic order close to superconductivity in the iron-based layered $LaO_{1-x}F_xFeAs$ systems, Nature 453 (2008) 899–902.
[5] M. Rotter, M. Tegel, D. Johrendt, I. Schellenberg, W. Hermes, R. Pöttgen, Spin-density-wave anomaly at 140 K in the ternary iron arsenide $BaFe_2As_2$, Phys. Rev. B 78 (2008) 020503.
[6] T. Nomura, S.W. Kim, Y. Kamihara, M. Hirano, P.V. Sushko, K. Kato, M. Takata, A.L. Shluger, H. Hosono, Crystallographic phase transition and high-T_c superconductivity in LaFeAsO:F, Supercond. Sci. Technol. 21 (2008) 125028.
[7] M.D. Lumsden, A.D. Christianson, Magnetism in Fe-based superconductors, J. Phys. Condens. Matter 22 (2010) 203203.
[8] A. Cano, M. Civelli, I. Eremin, I. Paul, Interplay of magnetic and structural transitions in iron-based pnictide superconductors, Phys. Rev. B 82 (2010) 020408.

[9] S. Avci, O. Chmaissem, E.A. Goremychkin, S. Rosenkranz, J.-P. Castellan, D.Y. Chung, I.S. Todorov, J.A. Schlueter, H. Claus, M.G. Kanatzidis, A. Daoud-Aladine, D. Khalyavin, R. Osborn, Magnetoelastic coupling in the phase diagram of $Ba_{1-x}K_xFe_2As_2$ as seen via neutron diffraction, Phys. Rev. B 83 (2011) 172503.

[10] M.G. Kim, R.M. Fernandes, A. Kreyssig, J.W. Kim, A. Thaler, S.L. Bud'ko, P.C. Canfield, R.J. McQueeney, J. Schmalian, A.I. Goldman, Character of the structural and magnetic phase transitions in the parent and electron-doped $BaFe_2As_2$ compounds, Phys. Rev. B 83 (2011) 134522.

[11] N. Ni, M.E. Tillman, J.-Q. Yan, A. Kracher, S.T. Hannahs, S.L. Bud'ko, P.C. Canfield, Effects of Co substitution on thermodynamic and transport properties and anisotropic H_{c2} in $Ba(Fe_{1-x}Co_x)_2As_2$ single crystals, Phys. Rev. B 78 (2008) 214515.

[12] J.-H. Chu, J.G. Analytis, C. Kucharczyk, I.R. Fisher, Determination of the phase diagram of the electron-doped superconductor $Ba(Fe_{1-x}Co_x)_2As_2$, Phys. Rev. B 79 (2009) 014506.

[13] C. Lester, J.-H. Chu, J.G. Analytis, S.C. Capelli, A.S. Erickson, C.L. Condron, M.F. Toney, I.R. Fisher, S.M. Hayden, Neutron scattering study of the interplay between structure and magnetism in $Ba(Fe_{1-x}Co_x)_2As_2$, Phys. Rev. B 79 (2009) 144523.

[14] A. Kreyssig, M.G. Kim, S. Nandi, D.K. Pratt, W. Tian, J.L. Zarestky, N. Ni, A. Thaler, S.L. Bud'ko, P.C. Canfield, R.J. McQueeney, A.I. Goldman, Suppression of antiferromagnetic order and orthorhombic distortion in superconducting $Ba(Fe_{0.0.961}Rh_{0.039})_2As_2$, Phys. Rev. B 81 (2010) 134512.

[15] N. Ni, A. Thaler, J.Q. Yan, A. Kracher, E. Colombier, S.L. Bud'ko, P.C. Canfield, S.T. Hannahs, Temperature versus doping phase diagrams for $Ba(Fe_{1-x}TM_x)_2As_2$ (TM = Ni, Cu, Cu/Co) single crystals, Phys. Rev. B 82 (2010) 024519.

[16] H. Luetkens, H.-H. Klauss, M. Kraken, F.J. Litterst, T. Dellmann, R. Klingeler, C. Hess, R. Khasanov, A. Amato, C. Baines, M. Kosmala, O.J. Schumann, M. Braden, J. Hamann-Borrero, N. Leps, A. Kondrat, G. Behr, J. Werner, B. Büchner, The electronic phase diagram of the $La(O_{1-x}F_x)FeAs$ superconductor, Nat. Mater. 8 (2009) 305–309.

[17] D.R. Parker, M.J.P. Smith, T. Lancaster, A.J. Steele, I. Franke, P.J. Baker, F.L. Pratt, M.J. Pitcher, S.J. Blundell, S.J. Clarke, Control of the competition between a magnetic phase and a superconducting phase in cobalt-doped and nickel-doped NaFeAs using electron count, Phys. Rev. Lett. 104 (2010) 057007.

[18] C. Xu, M. Müller, S. Sachdev, Ising and spin orders in the iron-based superconductors, Phys. Rev. B 78 (2008) 020501.

[19] C. Fang, H. Yao, W.-F. Tsai, J. Hu, S.A. Kivelson, Theory of electron nematic order in LaFeAsO, Phys. Rev. B 77 (2008) 224509.

[20] S. Nandi, M.G. Kim, A. Kreyssig, R.M. Fernandes, D.K. Pratt, A. Thaler, N. Ni, S.L. Bud'ko, P.C. Canfield, J. Schmalian, R.J. McQueeney, A.I. Goldman, Anomalous suppression of the orthorhombic lattice distortion in superconducting $Ba(Fe_{1-x}Co_x)_2As_2$ single crystals, Phys. Rev. Lett. 104 (2010) 057006.

[21] R.M. Fernandes, L.H. VanBebber, S. Bhattacharya, P. Chandra, V. Keppens, D. Mandrus, M.A. McGuire, B.C. Sales, A.S. Sefat, J. Schmalian, Effects of nematic fluctuations on the elastic properties of iron arsenide superconductors, Phys. Rev. Lett. 105 (2010) 157003.

[22] T.M. McQueen, A.J. Williams, P.W. Stephens, J. Tao, Y. Zhu, V. Ksenofontov, F. Casper, C. Felser, R.J. Cava, Tetragonal-to-orthorhombic structural phase transition at 90 K in the superconductor $Fe_{1.01}Se$, Phys. Rev. Lett. 103 (2009) 057002.

[23] A.E. Böhmer, P. Burger, F. Hardy, T. Wolf, P. Schweiss, R. Fromknecht, M. Reinecker, W. Schranz, C. Meingast, Nematic susceptibility of hole-doped and electron-doped $BaFe_2As_2$ iron-based superconductors from shear modulus measurements, Phys. Rev. Lett. 112 (2014) 047001.

[24] A.E. Böhmer, Competing phases in iron-based superconductors studied by high-resolution thermal-expansion and shear-modulus measurements, Ph.D. thesis, Diss., Fakultät für Physik, Karlsruhe Institute of Technology (KIT), Karlsruhe, 2014, http://digbib.ubka.uni-karlsruhe.de/volltexte/1000042623.

[25] J.-H. Chu, H.-H. Kuo, J.G. Analytis, I.R. Fisher, Divergent nematic susceptibility in an iron arsenide superconductor, Science 337 (2012) 710–712.

[26] R.M. Fernandes, A.E. Böhmer, C. Meingast, J. Schmalian, Scaling between magnetic and lattice fluctuations in iron pnictide superconductors, Phys. Rev. Lett. 111 (2013) 137001.

[27] A.E. Böhmer, T. Arai, F. Hardy, T. Hattori, T. Iye, T. Wolf, H.v. Löhneysen, K. Ishida, C. Meingast, Origin of the tetragonal-to-orthorhombic phase transition in FeSe: a combined thermodynamic and NMR study of nematicity, Phys. Rev. Lett. 114 (2015) 027001.

[28] J.-H. Chu, J.G. Analytis, K. De Greve, P.L. McMahon, Z. Islam, Y. Yamamoto, I.R. Fisher, In-plane resistivity anisotropy in an underdoped iron arsenide superconductor, Science 329 (2010) 824–826.

[29] J.J. Ying, X.F. Wang, T. Wu, Z.J. Xiang, R.H. Liu, Y.J. Yan, A.F. Wang, M. Zhang, G.J. Ye, P. Cheng, J.P. Hu, X.H. Chen, Measurements of the anisotropic in-plane resistivity of underdoped FeAs-based pnictide superconductors, Phys. Rev. Lett. 107 (2011) 067001.

[30] M. Nakajima, S. Ishida, Y. Tomioka, K. Kihou, C.H. Lee, A. Iyo, T. Ito, T. Kakeshita, H. Eisaki, S. Uchida, Effect of Co doping on the in-plane anisotropy in the optical spectrum of underdoped $Ba(Fe_{1-x}Co_x)_2As_2$, Phys. Rev. Lett. 109 (2012) 217003.

[31] S. Ishida, M. Nakajima, T. Liang, K. Kihou, C.H. Lee, A. Iyo, H. Eisaki, T. Kakeshita, Y. Tomioka, T. Ito, S. Uchida, Anisotropy of the in-plane resistivity of underdoped $Ba(Fe_{1-x}Co_x)_2As_2$ superconductors induced by impurity scattering in the antiferromagnetic orthorhombic phase, Phys. Rev. Lett. 110 (2013) 207001.

[32] S. Ishida, M. Nakajima, T. Liang, K. Kihou, C.-H. Lee, A. Iyo, H. Eisaki, T. Kakeshita, Y. Tomioka, T. Ito, S.-i. Uchida, Effect of doping on the magnetostructural ordered phase of iron arsenides: a comparative study of the resistivity anisotropy in doped $BaFe_2As_2$ with doping into three different sites, J. Am. Chem. Soc. 135 (2013) 3158–3163.

[33] E.C. Blomberg, M.A. Tanatar, R.M. Fernandes, I.I. Mazin, B. Shen, H.-H. Wen, M.D. Johannes, J. Schmalian, R. Prozorov, Sign-reversal of the in-plane resistivity anisotropy in hole-doped iron pnictides, Nat. Commun. 4 (2013), Art. No. 1914.

[34] L. Liu, T. Mikami, S. Ishida, K. Koshiishi, K. Okazaki, T. Yoshida, H. Suzuki, M. Horio, L.C.C. Ambolode II, J. Xu, H. Kumigashira, K. Ono, M. Nakajima, K. Kihou, C.H. Lee, A. Iyo, H. Eisaki, T. Kakeshita, S. Uchida, A. Fujimori, In-plane electronic anisotropy in the antiferromagnetic-orthorhombic phase of isovalent-substituted $Ba(Fe_{1-x}Ru_x)_2As_2$, arXiv:1503.02855, 2015.

[35] R.M. Fernandes, E. Abrahams, J. Schmalian, Anisotropic in-plane resistivity in the nematic phase of the iron pnictides, Phys. Rev. Lett. 107 (2011) 217002.

[36] M.N. Gastiasoro, I. Paul, Y. Wang, P.J. Hirschfeld, B.M. Andersen, Emergent defect states as a source of resistivity anisotropy in the nematic phase of iron pnictides, Phys. Rev. Lett. 113 (2014) 127001.

[37] C.-L. Song, Y.-L. Wang, Y.-P. Jiang, L. Wang, K. He, X. Chen, J.E. Hoffman, X.-C. Ma, Q.-K. Xue, Suppression of superconductivity by twin boundaries in FeSe, Phys. Rev. Lett. 109 (2012) 137004.

[38] M.P. Allan, T.-M. Chuang, F. Massee, Y. Xie, N. Ni, S.L. Bud/'ko, G.S. Boebinger, Q. Wang, D.S. Dessau, P.C. Canfield, M.S. Golden, J.C. Davis, Anisotropic impurity states, quasiparticle scattering and nematic transport in underdoped $Ca(Fe_{1-x}Co_x)_2As_2$, Nat. Phys. 9 (2013) 220–224.

[39] E.P. Rosenthal, E.F. Andrade, C.J. Arguello, R.M. Fernandes, L.Y. Xing, X.C. Wang, C.Q. Jin, A.J. Millis, A.N. Pasupathy, Visualization of electron nematicity and unidirectional antiferroic fluctuations at high temperatures in NaFeAs, Nat. Phys. 10 (2014) 225–232.

[40] Q. Deng, J. Xing, J. Liu, H. Yang, H.-H. Wen, Anisotropic electronic mobilities in the nematic state of the parent phase NaFeAs, arXiv:1503.07090, 2015.

[41] A. Dusza, A. Lucarelli, F. Pfuner, J.-H. Chu, I.R. Fisher, L. Degiorgi, Anisotropic charge dynamics in detwinned $Ba(Fe_{1-x}Co_x)_2As_2$, Europhys. Lett. 93 (2011) 37002.

[42] C. Mirri, A. Dusza, S. Bastelberger, J.-H. Chu, H.-H. Kuo, I.R. Fisher, L. Degiorgi, Hysteretic behavior in the optical response of the underdoped Fe-arsenide $Ba(Fe_{1-x}Co_x)_2As_2$ in the electronic nematic phase, Phys. Rev. B 89 (2014) 060501.

[43] C. Mirri, A. Dusza, S. Bastelberger, J.-H. Chu, H.-H. Kuo, I.R. Fisher, L. Degiorgi, Nematic-driven anisotropic electronic properties of underdoped detwinned $Ba(Fe_{1-x}Co_x)_2As_2$ revealed by optical spectroscopy, Phys. Rev. B 90 (2014) 155125.

[44] C. Mirri, A. Dusza, S. Bastelberger, M. Chinotti, J.-H. Chu, H.-H. Kuo, I.R. Fisher, L. Degiorgi, Origin of the resistive anisotropy in the electronic nematic phase of $BaFe_2As_2$ revealed by optical spectroscopy, arXiv:1504.06829, 2015.

[45] H. Kuo, I.R. Fisher, Effect of disorder on the resistivity anisotropy near the electronic nematic phase transition in pure and electron-doped $BaFe_2As_2$, Phys. Rev. Lett. 112 (2014) 227001.

[46] M. Yi, D. Lu, J.-H. Chu, J.G. Analytis, A.P. Sorini, A.F. Kemper, B. Moritz, S.-K. Mo, R.G. Moore, M. Hashimoto, W.-S. Lee, Z. Hussain, T.P. Devereaux, I.R. Fisher, Z.-X. Shen, Symmetry-breaking orbital anisotropy observed for detwinned $Ba(Fe_{1-x}Co_x)_2As_2$ above the spin density wave transition, Proc. Natl. Acad. Sci. USA 108 (2011) 6878–6883.
[47] B. Valenzuela, E. Bascones, M.J. Calderón, Conductivity anisotropy in the antiferromagnetic state of iron pnictides, Phys. Rev. Lett. 105 (2010) 207202.
[48] M. Daghofer, Q.-L. Luo, R. Yu, D.X. Yao, A. Moreo, E. Dagotto, Orbital-weight redistribution triggered by spin order in the pnictides, Phys. Rev. B 81 (2010) 180514.
[49] Z.P. Yin, K. Haule, G. Kotliar, Magnetism and charge dynamics in iron pnictides, Nat. Phys. 7 (2011) 294–297.
[50] S. Jiang, H.S. Jeevan, J. Dong, P. Gegenwart, Thermopower as a sensitive probe of electronic nematicity in iron pnictides, Phys. Rev. Lett. 110 (2013) 067001.
[51] M. Fu, D.A. Torchetti, T. Imai, F.L. Ning, J.-Q. Yan, A.S. Sefat, NMR search for the spin nematic state in a LaFeAsO single crystal, Phys. Rev. Lett. 109 (2012) 247001.
[52] L.W. Harriger, H.Q. Luo, M.S. Liu, C. Frost, J.P. Hu, M.R. Norman, P. Dai, Nematic spin fluid in the tetragonal phase of $BaFe_2As_2$, Phys. Rev. B 84 (2011) 054544.
[53] X. Lu, J.T. Park, R. Zhang, H. Luo, A.H. Nevidomskyy, Q. Si, P. Dai, Nematic spin correlations in the tetragonal state of uniaxial-strained $BaFe_{2-x}Ni_xAs_2$, Science 345 (2014) 657–660.
[54] D. Inosov, Spin fluctuations in iron pnictides and chalcogenides: from antiferromagnetism to superconductivity, C. R. Phys. 16 (2015) (this issue).
[55] A. Patz, T. Li, S. Ran, R.M. Fernandes, J. Schmalian, S.L. Bud'ko, P.C. Canfield, I.E. Perakis, J. Wang, Ultrafast observation of critical nematic fluctuations and giant magnetoelastic coupling in iron pnictides, Nat. Commun. 5 (2014), Article No. 3229.
[56] I.R. Fisher, L. Degiorgi, Z.X. Shen, In-plane electronic anisotropy of underdoped '122' Fe-arsenide superconductors revealed by measurements of detwinned single crystals, Rep. Prog. Phys. 74 (2011) 124506.
[57] J.P.C. Ruff, J.-H. Chu, H.-H. Kuo, R.K. Das, H. Nojiri, I.R. Fisher, Z. Islam, Susceptibility anisotropy in an iron arsenide superconductor revealed by X-ray diffraction in pulsed magnetic fields, Phys. Rev. Lett. 109 (2012) 027004.
[58] S. Zapf, C. Stingl, K.W. Post, J. Maiwald, N. Bach, I. Pietsch, D. Neubauer, A. Löhle, C. Clauss, S. Jiang, H.S. Jeevan, D.N. Basov, P. Gegenwart, M. Dressel, Persistent detwinning of iron-pnictide $EuFe_2As_2$ crystals by small external magnetic fields, Phys. Rev. Lett. 113 (2014) 227001.
[59] E.C. Blomberg, A. Kreyssig, M.A. Tanatar, R.M. Fernandes, M.G. Kim, A. Thaler, J. Schmalian, S.L. Bud'ko, P.C. Canfield, A.I. Goldman, R. Prozorov, Effect of tensile stress on the in-plane resistivity anisotropy in $BaFe_2As_2$, Phys. Rev. B 85 (2012) 144509.
[60] C. Dhital, Z. Yamani, W. Tian, J. Zeretsky, A.S. Sefat, Z. Wang, R.J. Birgeneau, S.D. Wilson, Effect of uniaxial strain on the structural and magnetic phase transitions in $BaFe_2As_2$, Phys. Rev. Lett. 108 (2012) 087001.
[61] J. Hu, C. Setty, S. Kivelson, Pressure effects on magnetically driven electronic nematic states in iron pnictide superconductors, Phys. Rev. B 85 (2012) 100507.
[62] X. Ren, L. Duan, Y. Hu, J. Li, R. Zhang, H. Luo, P. Dai, Y. Li, Nematic crossover in $BaFe_2As_2$ under uniaxial stress, arXiv:1507.02080, 2015, arXiv e-prints.
[63] Y. Gallais, R.M. Fernandes, I. Paul, L. Chauvière, Y.-X. Yang, M.-A. Méasson, M. Cazayous, A. Sacuto, D. Colson, A. Forget, Observation of incipient charge nematicity in $Ba(Fe_{1-x}Co_x)_2As_2$, Phys. Rev. Lett. 111 (2013) 267001.
[64] H. Kontani, T. Saito, S. Onari, Origin of orthorhombic transition, magnetic transition, and shear-modulus softening in iron pnictide superconductors: analysis based on the orbital fluctuations theory, Phys. Rev. B 84 (2011) 024528.
[65] H. Yamase, R. Zeyher, Superconductivity from orbital nematic fluctuations, Phys. Rev. B 88 (2013) 180502.
[66] M. Yoshizawa, S. Simayi, Anomalous elastic behavior and its correlation with superconductivity in iron-based superconductor $Ba(Fe_{1-x}Co_x)_2As_2$, Mod. Phys. Lett. B 26 (2012) 1230011.
[67] S. Margadonna, Y. Takabayashi, Y. Ohishi, Y. Mizuguchi, Y. Takano, T. Kagayama, T. Nakagawa, M. Takata, K. Prassides, Pressure evolution of the low-temperature crystal structure and bonding of the superconductor FeSe ($T_c = 37$ K), Phys. Rev. B 80 (2009) 064506.
[68] M. Bendele, A. Amato, K. Conder, M. Elender, H. Keller, H.-H. Klauss, H. Luetkens, E. Pomjakushina, A. Raselli, R. Khasanov, Pressure induced static magnetic order in superconducting $FeSe_{1-x}$, Phys. Rev. Lett. 104 (2010) 087003.
[69] T. Imai, K. Ahilan, F.L. Ning, T.M. McQueen, R.J. Cava, Why does undoped FeSe become a high-T_c superconductor under pressure?, Phys. Rev. Lett. 102 (2009) 177005.
[70] A.E. Böhmer, F. Hardy, F. Eilers, D. Ernst, P. Adelmann, P. Schweiss, T. Wolf, C. Meingast, Lack of coupling between superconductivity and orthorhombic distortion in stoichiometric single-crystalline FeSe, Phys. Rev. B 87 (2013) 180505.
[71] J.-Y. Lin, Y.S. Hsieh, D.A. Chareev, A.N. Vasiliev, Y. Parsons, H.D. Yang, Coexistence of isotropic and extended s-wave order parameter in FeSe as revealed by low-temperature specific heat, Phys. Rev. B 84 (2011) 220507(R).
[72] D. Chareev, E. Osadchii, T. Kuzmicheva, J.-Y. Lin, S. Kuzmichev, O. Volkova, A. Vasiliev, Single crystal growth and characterization of tetragonal $FeSe_{1-x}$ superconductors, CrystEngComm 15 (2013) 1989–1993.
[73] S.-H. Baek, D.V. Efremov, J.M. Ok, J.S. Kim, J. van den Brink, B. Büchner, Orbital-driven nematicity in FeSe, Nat. Mater. 14 (2015) 210–214.
[74] M.D. Watson, T.K. Kim, A.A. Haghighirad, N.R. Davies, A. McCollam, A. Narayanan, S.F. Blake, Y.L. Chen, S. Ghannadzadeh, A.J. Schofield, M. Hoesch, C. Meingast, T. Wolf, A.I. Coldea, Emergence of the nematic electronic state in FeSe, Phys. Rev. B 91 (2015) 155106.
[75] T. Shimojima, Y. Suzuki, T. Sonobe, A. Nakamura, M. Sakano, J. Omachi, K. Yoshioka, M. Kuwata-Gonokami, K. Ono, H. Kumigashira, A.E. Böhmer, F. Hardy, T. Wolf, C. Meingast, H.v. Löhneysen, H. Ikeda, K. Ishizaka, Lifting of xz/yz orbital degeneracy at the structural transition in detwinned FeSe, Phys. Rev. B 90 (2014) 121111.
[76] J. Maletz, V.B. Zabolotnyy, D.V. Evtushinsky, S. Thirupathaiah, A.U.B. Wolter, L. Harnagea, A.N. Yaresko, A.N. Vasiliev, D.A. Chareev, A.E. Böhmer, F. Hardy, T. Wolf, C. Meingast, E.D.L. Rienks, B. Büchner, S.V. Borisenko, Unusual band renormalization in the simplest iron-based superconductor $FeSe_{1-x}$, Phys. Rev. B 89 (2014) 220506.
[77] K. Nakayama, Y. Miyata, G. Phan, T. Sato, Y. Tanabe, T. Urata, K. Tanigaki, T. Takahashi, Reconstruction of band structure induced by electronic nematicity in an FeSe superconductor, Phys. Rev. Lett. 113 (2014) 237001.
[78] M.C. Rahn, R.A. Ewings, S.J. Sedlmaier, S.J. Clarke, A.T. Boothroyd, Strong $(\pi, 0)$ spin fluctuations in β-FeSe observed by neutron spectroscopy, Phys. Rev. B 91 (2015) 180501.
[79] Q. Wang, Y. Shen, B. Pan, Y. Hao, M. Ma, F. Zhou, P. Steffens, K. Schmalzl, T.R. Forrest, M. Abdel-Hafiez, D.A. Chareev, A.N. Vasiliev, P. Bourges, Y. Sidis, H. Cao, J. Zhao, Strong interplay between stripe spin fluctuations, nematicity and superconductivity in FeSe, arXiv:1502.07544, 2015.
[80] G. Garbarino, A. Sow, P. Lejay, A. Sulpice, P. Toulemonde, M. Mezouar, M. Núñez-Regueiro, High-temperature superconductivity (T_c onset at 34 K) in the high-pressure orthorhombic phase of FeSe, Europhys. Lett. 86 (2009) 27001.
[81] M. Bendele, A. Ichsanow, Y. Pashkevich, L. Keller, T. Strässle, A. Gusev, E. Pomjakushina, K. Conder, R. Khasanov, H. Keller, Coexistence of superconductivity and magnetism in $FeSe_{1-x}$ under pressure, Phys. Rev. B 85 (2012) 064517.
[82] K. Miyoshi, K. Morishita, E. Mutou, M. Kondo, O. Seida, K. Fujiwara, J. Takeuchi, S. Nishigori, Enhanced superconductivity on the tetragonal lattice in FeSe under hydrostatic pressure, J. Phys. Soc. Jpn. 83 (2014) 013702.
[83] T. Terashima, N. Kikugawa, S. Kasahara, T. Watashige, T. Shibauchi, Y. Matsuda, T. Wolf, A.E. Böhmer, F. Hardy, C. Meingast, H.v. Löhneysen, S. Uji, Pressure-induced antiferromagnetic transition and phase diagram in FeSe, J. Phys. Soc. Jpn. 84 (2015) 063701.
[84] S. Knöner, D. Zielke, S. Köhler, B. Wolf, T. Wolf, L. Wang, A. Böhmer, C. Meingast, M. Lang, Resistivity and magnetoresistance of FeSe single crystals under helium-gas pressure, Phys. Rev. B 91 (2015) 174510.

[85] Y. Mizuguchi, F. Tomioka, S. Tsuda, T. Yamaguchi, Y. Takano, Superconductivity at 27 K in tetragonal FeSe under high pressure, Appl. Phys. Lett. 93 (2008) 152505.
[86] S. Medvedev, T.M. McQueen, I.A. Troyan, T. Palasyuk, M.I. Eremets, R.J. Cava, S. Naghavi, F. Casper, V. Ksenofontov, G. Wortmann, C. Felser, Electronic and magnetic phase diagram of β-$Fe_{1.01}$ with superconductivity at 36.7 K under pressure, Nat. Mater. 8 (2009) 630–633.
[87] R. Yu, Q. Si, Antiferroquadrupolar and Ising-nematic orders of a frustrated bilinear–biquadratic Heisenberg model and implications for the magnetism of FeSe, arXiv:1501.05926, 2015.
[88] J.K. Glasbrenner, I.I. Mazin, H.O. Jeschke, P.J. Hirschfeld, R. Valentí, Effect of magnetic frustration on nematicity and superconductivity in Fe chalcogenides, arXiv:1501.04946, 2015.
[89] F. Wang, S. Kivelson, D.-H. Lee, Is FeSe a nematic quantum paramagnet?, arXiv:1501.00844, 2015.
[90] S. Mukherjee, A. Kreisel, P.J. Hirschfeld, B. Andersen, Model of electronic structure and superconductivity in orbitally ordered FeSe, arXiv:1502.03354, 2015.
[91] A.V. Chubukov, R.M. Fernandes, J. Schmalian, The origin of nematic order in FeSe, arXiv:1504.02315, 2015.
[92] S. Avci, O. Chmaissem, J. Allred, S. Rosenkranz, I. Eremin, A. Chubukov, D. Bugaris, D. Chung, M. Kanatzidis, J.-P. Castellan, J. Schlueter, H. Claus, D. Khalyavin, P. Manuel, A. Daoud-Aladine, R. Osborn, Magnetically driven suppression of nematic order in an iron-based superconductor, Nat. Commun. 5 (2014) 3845.
[93] F. Waßer, A. Schneidewind, Y. Sidis, S. Wurmehl, S. Aswartham, B. Büchner, M. Braden, Spin reorientation in $Ba_{0.65}Na_{0.35}Fe_2As_2$ studied by single-crystal neutron diffraction, Phys. Rev. B 91 (2015) 060505.
[94] D.D. Khalyavin, S.W. Lovesey, P. Manuel, F. Krüger, S. Rosenkranz, J.M. Allred, O. Chmaissem, R. Osborn, Symmetry of reentrant tetragonal phase in $Ba_{1-x}Na_xFe_2As_2$: Magnetic versus orbital ordering mechanism, Phys. Rev. B 90 (2014) 174511.
[95] J. Kang, X. Wang, A.V. Chubukov, R.M. Fernandes, Interplay between tetragonal magnetic order, stripe magnetism, and superconductivity in iron-based materials, Phys. Rev. B 91 (2015) 121104.
[96] M.N. Gastiasoro, B.M. Andersen, Competing magnetic double-Q phases and superconductivity-induced re-entrance of C_2 magnetic stripe order in iron pnictides, arXiv:1502.05859, 2015.
[97] K.M. Taddei, et al., in: APS March Meeting 2015, Abstract L5.00006, 2015.
[98] A.E. Böhmer, F. Hardy, L. Wang, T. Wolf, P. Schweiss, C. Meingast, Superconductivity-induced reentrance of orthorhombic distortion in $Ba_{1-x}K_xFe_2As_2$, arXiv:1412.7038, 2014.
[99] E. Salje, Phase Transitions in Ferroelastic and Co-Elastic Crystals, Cambridge University Press, 1993, http://www.cambridge.org/ve/academic/subjects/earth-and-environmental-science/mineralogy-petrology-and-volcanology/phase-transitions-ferroelastic-and-co-elastic-crystals.
[100] T. Goto, R. Kurihara, K. Araki, K. Mitsumoto, M. Akatsu, Y. Nemoto, S. Tatematsu, M. Sato, Quadrupole effects in layered iron pnictide superconductor $Ba(Fe_{0.9}Co_{0.1})_2As_2$, J. Phys. Soc. Jpn. 80 (2011) 073702.
[101] M. Yoshizawa, D. Kimura, T. Chiba, S. Simayi, Y. Nakanishi, K. Kihou, C.-H. Lee, A. Iyo, H. Eisaki, M. Nakajima, S.-i. Uchida, Structural quantum criticality and superconductivity in iron-based superconductor $Ba(Fe_{1-x}Co_x)_2As_2$, J. Phys. Soc. Jpn. 81 (2012) 024604.
[102] S. Simayi, K. Sakano, H. Takezawa, M. Nakamura, Y. Nakanishi, K. Kihou, M. Nakajima, C.-H. Lee, A. Iyo, H. Eisaki, S. ichi Uchida, M. Yoshizawa, Strange inter-layer properties of $Ba(Fe_{1-x}Co_x)_2As_2$ appearing in ultrasonic measurements, J. Phys. Soc. Jpn. 82 (2013) 114604.
[103] G.A. Zvyagina, T.N. Gaydamak, K.R. Zhekov, I.V. Bilich, V.D. Fil, D.A. Chareev, A.N. Vasiliev, Acoustic characteristics of FeSe single crystals, Europhys. Lett. 101 (2013) 56005.
[104] S. Liang, A. Moreo, E. Dagotto, Nematic state of pnictides stabilized by interplay between spin, orbital, and lattice degrees of freedom, Phys. Rev. Lett. 111 (2013) 047004.
[105] S. Liang, A. Mukherjee, N.D. Patel, C.B. Bishop, E. Dagotto, A. Moreo, Diverging nematic susceptibility, physical meaning of T^* scale, and pseudogap in the spin fermion model for the pnictides, Phys. Rev. B 90 (2014) 184507.
[106] W. Rehwald, The study of structural phase transitions by means of ultrasonic experiments, Adv. Phys. 22 (1973) 721–755.
[107] J.-P. Benoît, J. Berger, M. Krauzman, J.L. Godet, Experimental observation of a soft mode in ammonium hydrogen oxalate hemihydrate by Brillouin scattering, J. Phys. France 47 (1986) 815–819.
[108] R.A. Cowley, Acoustic phonon instabilities and structural phase transitions, Phys. Rev. B 13 (1976) 4877–4885.
[109] R. Folk, H. Iro, F. Schwabl, Critical statics of elastic phase transitions, Z. Phys. B, Condens. Matter 25 (1976) 69–81.
[110] J. Als-Nielsen, R.J. Birgeneau, Mean field theory, the Ginzburg criterion, and marginal dimensionality of phase transitions, Am. J. Phys. 45 (1977) 554–560.
[111] A.V. Kityk, V.P. Soprunyuk, A. Fuith, W. Schranz, H. Warhanek, Low-frequency elastic properties of the incommensurate ferroelastic $[N(CH_3)_4]_2CuCl_4$, Phys. Rev. B 53 (1996) 6337–6344.
[112] B.W. Rossiter, R.C. Baetzold (Eds.), Physical Methods of Chemistry, vol. 7, Wiley, New York, N.Y., 1991, http://eu.wiley.com/WileyCDA/WileyTitle/productCd-0471534382.html.
[113] C. Meingast, B. Blank, H. Bürkle, B. Obst, T. Wolf, H. Wühl, V. Selvamanickam, K. Salama, Anisotropic pressure dependence of T_c in single crystal $YBa_2Cu_3O_7$ via thermal expansion, Phys. Rev. B 41 (1990) 11299–11304.
[114] C. Meingast, F. Hardy, R. Heid, P. Adelmann, A. Böhmer, P. Burger, D. Ernst, R. Fromknecht, P. Schweiss, T. Wolf, Thermal expansion and Grüneisen parameters of $Ba(Fe_{1-x}Co_x)_2As_2$—a thermodynamic quest for quantum criticality, Phys. Rev. Lett. 108 (2012) 177004.
[115] E.K.H. Salje, W. Schranz, Low amplitude, low frequency elastic measurements using dynamic mechanical analyzer (DMA) spectroscopy, Z. Kristallogr. 226 (2010) 1–17.
[116] Currently unpublished, measurements were made in Prof. W. Schranz's group in Vienna, 2015.
[117] D. Parshall, L. Pintschovius, J.L. Niedziela, J.-P. Castellan, D. Lamago, R. Mittal, T. Wolf, D. Reznik, Close correlation between magnetic properties and the soft phonon mode of the structural transition in $BaFe_2As_2$ and $SrFe_2As_2$, Phys. Rev. B 91 (2015) 134426.
[118] W. Schranz, H. Kabelka, A. Sarras, M. Burock, Giant domain wall response of highly twinned ferroelastic materials, Appl. Phys. Lett. 101 (2012) 141913.
[119] W. Schranz, H. Kabelka, A. Tröster, Superelastic softening of ferroelastic multidomain crystals, Ferroelectrics 426 (2012) 242–250.
[120] Y.P. Varshni, Temperature dependence of the elastic constants, Phys. Rev. B 2 (1970) 3952–3958.
[121] S. Kasahara, H.J. Shi, K. Hashimoto, S. Tonegawa, Y. Mizukami, T. Shibauchi, K. Sugimoto, T. Fukuda, T. Terashima, A.H. Nevimdomskyy, Y. Matsuda, Electronic nematicity above the structural and superconducting transition in $BaFe_2(As_{1-x}P_2)_2$, Nature 486 (2012) 382.
[122] A.E. Böhmer, P. Burger, F. Hardy, T. Wolf, P. Schweiss, R. Fromknecht, H.v. Löhneysen, C. Meingast, H.K. Mak, R. Lortz, S. Kasahara, T. Terashima, T. Shibauchi, Y. Matsuda, Thermodynamic phase diagram, phase competition, and uniaxial pressure effects in $BaFe_2(As_{1-x}P_x)_2$ studied by thermal expansion, Phys. Rev. B 86 (2012) 094521.
[123] X. Luo, V. Stanev, B. Shen, L. Fang, X.S. Ling, R. Osborn, S. Rosenkranz, T.M. Benseman, R. Divan, W.-K. Kwok, U. Welp, Antiferromagnetic and nematic phase transitions in $BaFe_2(As_{1-x}P_x)_2$ studied by ac microcalorimetry and SQUID magnetometry, Phys. Rev. B 91 (2015) 094512.
[124] H. Kontani, Y. Yamakawa, Linear response theory for shear modulus C_{66} and Raman quadrupole susceptibility: evidence for nematic orbital fluctuations in Fe-based superconductors, Phys. Rev. Lett. 113 (2014) 047001.
[125] A. Pippard, CXXIII. Thermodynamics of a sheared superconductor, Lond. Edinb. Dublin Philos. Mag. J. Sci. 46 (1955) 1115–1118.
[126] R.M. Fernandes, A.J. Millis, Nematicity as a probe of superconducting pairing in iron-based superconductors, Phys. Rev. Lett. 111 (2013) 127001.

[127] T. Terashima, N. Kikugawa, A. Kiswandhi, E.-S. Choi, J.S. Brooks, S. Kasahara, T. Watashige, H. Ikeda, T. Shibauchi, Y. Matsuda, T. Wolf, A.E. Böhmer, F. Hardy, C. Meingast, H.v. Löhneysen, M.-T. Suzuki, R. Arita, S. Uji, Anomalous Fermi surface in FeSe seen by Shubnikov–de Haas oscillation measurements, Phys. Rev. B 90 (2014) 144517.
[128] S. Kasahara, T. Watashige, T. Hanaguri, Y. Kohsaka, T. Yamashita, Y. Shimoyama, Y. Mizukami, R. Endo, H. Ikeda, K. Aoyama, T. Terashima, S. Uji, T. Wolf, H. von Löhneysen, T. Shibauchi, Y. Matsuda, Field-induced superconducting phase of FeSe in the BCS–BEC cross-over, Proc. Natl. Acad. Sci. USA 111 (2014) 16309–16313.
[129] F. Hardy, et al., 2015 (in preparation).
[130] F. Hardy, T. Wolf, R.A. Fisher, R. Eder, P. Schweiss, P. Adelmann, H.v. Löhneysen, C. Meingast, Calorimetric evidence of multiband superconductivity in $Ba(Fe_{0.925}Co_{0.075})_2As_2$ single crystals, Phys. Rev. B 81 (2010) 060501.
[131] C. Meingast, 2015 (currently unpublished).
[132] F. Hardy, P. Burger, T. Wolf, R.A. Fisher, P. Schweiss, P. Adelmann, R. Heid, R. Fromknecht, R. Eder, D. Ernst, H.v. Löhneysen, C. Meingast, Doping evolution of superconducting gaps and electronic densities of states in $Ba(Fe_{1-x}Co_x)_2As_2$ iron pnictides, Europhys. Lett. 91 (2010) 47008.
[133] H.-H. Kuo, M.C. Shapiro, S.C. Riggs, I.R. Fisher, Measurement of the elastoresistivity coefficients of the underdoped iron arsenide $Ba(Fe_{0.975}Co_{0.025})_2As_2$, Phys. Rev. B 88 (2013) 085113.
[134] H.-H. Kuo, J.-H. Chu, S.A. Kivelson, I.R. Fisher, Ubiquitous signatures of nematic quantum criticality in optimally doped Fe-based superconductors, arXiv:1503.00402, 2015.
[135] Y.-X. Yang, Y. Gallais, R.M. Fernandes, I. Paul, L. Chauvière, M.-A. Méasson, M. Cazayous, A. Sacuto, D. Colson, A. Forget, Raman scattering as a probe of charge nematic fluctuations in iron based superconductors, JPS Conf. Proc. 3 (2013) 015001.
[136] Y. Gallais, in: APS March Meeting, 2015, Abstract Y51.00003.
[137] Y. Gallais, Private communication, 2015.
[138] Y. Gallais, I. Paul, Charge nematicity and electronic Raman scattering in iron-based superconductors, C. R. Physique 17 (1–2) (2016) 113–139, this issue.
[139] F.L. Ning, K. Ahilan, T. Imai, A.S. Sefat, M.A. McGuire, B.C. Sales, D. Mandrus, P. Cheng, B. Shen, H.-H. Wen, Contrasting spin dynamics between underdoped and overdoped $Ba(Fe_{1-x}Co_x)_2As_2$, Phys. Rev. Lett. 104 (2010) 037001.
[140] F.L. Ning, M. Fu, D.A. Torchetti, T. Imai, A.S. Sefat, P. Cheng, B. Shen, H.-H. Wen, Critical behavior of the spin density wave transition in underdoped $Ba(Fe_{1-x}Co_x)_2As_2$ ($x \leq 0.05$): ^{75}As NMR investigation, Phys. Rev. B 89 (2014) 214511.
[141] A. Smerald, N. Shannon, Angle-resolved NMR: quantitative theory of ^{75}As T_1 relaxation rate in $BaFe_2As_2$, Phys. Rev. B 84 (2011) 184437.
[142] M. Hirano, Y. Yamada, T. Saito, R. Nagashima, T. Konishi, T. Toriyama, Y. Ohta, H. Fukazawa, Y. Kohori, Y. Furukawa, K. Kihou, C.-H. Lee, A. Iyo, H. Eisaki, Potential antiferromagnetic fluctuations in hole-doped iron-pnictide superconductor $Ba_{1-x}K_xFe_2As_2$ studied by ^{75}As nuclear magnetic resonance measurement, J. Phys. Soc. Jpn. 81 (2012) 054704.
[143] Y. Nakai, T. Iye, S. Kitagawa, K. Ishida, S. Kasahara, T. Shibauchi, Y. Matsuda, H. Ikeda, T. Terashima, Normal-state spin dynamics in the iron-pnictide superconductors $BaFe_2(As_{1-x}P_x)_2$ and $Ba(Fe_{1-x}Co_x)_2As_2$ probed with NMR measurements, Phys. Rev. B 87 (2013) 174507.
[144] B. Sales, M. McGuire, A. Sefat, D. Mandrus, A semimetal model of the normal state magnetic susceptibility and transport properties of $Ba(Fe_{1?x}Co_x)_2As_2$, Physica C, Supercond. 470 (2010) 304–308.
[145] M. Ma, D. Yuan, Y. Wu, H. Zhou, X. Dong, F. Zhou, Flux-free growth of large superconducting crystal of FeSe by traveling-solvent floating-zone technique, Supercond. Sci. Technol. 27 (2014) 122001.
[146] Y. Gallais, I. Paul, L. Chauviere, J. Schmalian, Nematic resonance in the Raman response of iron-based superconductors, arXiv:1504.04570, 2015.
[147] S. Lederer, Y. Schattner, E. Berg, S.A. Kivelson, Enhancement of superconductivity near a nematic quantum critical point, Phys. Rev. Lett. 114 (2015) 097001.